A UNITED STATES DEPARTMENT OF COMMERCE PUBLICATION

SECTION A

JOURNAL OF RESEARCH

of the NATIONAL BUREAU OF STANDARDS

Volume 75A, Number 2 Mar.-Apr. 1971

Physics and Chemistry

U.S. DEPARTMENT OF COMMERCE National Bureau of Standards

Journal of Research

of the

National Bureau of Standards

A. Physics and Chemistry

Mar.–Apr. • 1971

VOLUME • 75A

NUMBER • 2

Editor: C. W. Beckett

Associate Editor: D. D. Wagman

Publication dates:
Feb. 1, Apr. 1, June 1, Aug. 1, Oct. 1, Dec. 1, 1971

J. Res. Nat. Bur. Stand. (U.S.), A
CODEN: JNBAA 75A (2) 877–97–104 (1971)

JOURNAL OF RESEARCH

The National Bureau of Standards Journal of Research reports research and development in the fields of activity shown at right. Also included from time to time are survey articles on topics closely related to the Bureau's scientific and technical program.

The Journal is published in three separate sections as follows:

A. Physics and Chemistry

Contains papers of interest primarily to scientists working in these fields. Issued six times a year. Annual subscription: domestic, $9.50; foreign, $11.75. Single copy, varies.

B. Mathematical Sciences

Presents studies and compilations designed mainly for the mathematician and the theoretical physicist. Issued quarterly. Annual subscription: domestic, $5.00; foreign, $6.25. Single copy, $1.25.

C. Engineering and Instrumentation

Reports research and development results of interest chiefly to the engineer and the applied scientist. Issued quarterly. Annual subscription: domestic, $5.00; foreign, $6.25. Single copy, $1.25.

The National Bureau of Standards[1] was established by an act of Congress March 3, 1901. The Bureau's overall goal is to strengthen and advance the Nation's science and technology and facilitate their effective application for public benefit. To this end, the Bureau conducts research and provides: (1) a basis for the Nation's physical measurement system, (2) scientific and technological services for industry and government, (3) a technical basis for equity in trade, and (4) technical services to promote public safety. The Bureau consists of the Institute for Basic Standards, the Institute for Materials Research, the Institute for Applied Technology, the Center for Computer Sciences and Technology, and the Office for Information Programs.

THE INSTITUTE FOR BASIC STANDARDS provides the central basis within the United States of a complete and consistent system of physical measurement; coordinates that system with measurement systems of other nations; and furnishes essential services leading to accurate and uniform physical measurements throughout the Nation's scientific community, industry, and commerce. The Institute consists of a Center for Radiation Research, an Office of Measurement Services and the following divisions:

Applied Mathematics—Electricity—Heat—Mechanics—Optical Physics—Linac Radiation[2]—Nuclear Radiation[2]—Applied Radiation[2]—Quantum Electronics[3]—Electromagnetics[3]—Time and Frequency[3]—Laboratory Astrophysics[3]—Cryogenics[3].

THE INSTITUTE FOR MATERIALS RESEARCH conducts materials research leading to improved methods of measurement, standards, and data on the properties of well-characterized materials needed by industry, commerce, educational institutions, and Government; provides advisory and research services to other Government agencies; and develops, produces, and distributes standard reference materials. The Institute consists of the Office of Standard Reference Materials and the following divisions:

Analytical Chemistry—Polymers—Metallurgy—Inorganic Materials—Reactor Radiation—Physical Chemistry.

THE INSTITUTE FOR APPLIED TECHNOLOGY provides technical services to promote the use of available technology and to facilitate technological innovation in industry and Government; cooperates with public and private organizations leading to the development of technological standards (including mandatory safety standards), codes and methods of test; and provides technical advice and services to Government agencies upon request. The Institute also monitors NBS engineering standards activities and provides liaison between NBS and national and international engineering standards bodies. The Institute consists of the following technical divisions and offices:

Engineering Standards Services—Weights and Measures—Flammable Fabrics—Invention and Innovation—Vehicle Systems Research—Product Evaluation Technology—Building Research—Electronic Technology—Technical Analysis—Measurement Engineering.

THE CENTER FOR COMPUTER SCIENCES AND TECHNOLOGY conducts research and provides technical services designed to aid Government agencies in improving cost effectiveness in the conduct of their programs through the selection, acquisition, and effective utilization of automatic data processing equipment; and serves as the principal focus within the executive branch for the development of Federal standards for automatic data processing equipment, techniques, and computer languages. The Center consists of the following offices and divisions:

Information Processing Standards—Computer Information—Computer Services—Systems Development—Information Processing Technology.

THE OFFICE FOR INFORMATION PROGRAMS promotes optimum dissemination and accessibility of scientific information generated within NBS and other agencies of the Federal Government; promotes the development of the National Standard Reference Data System and a system of information analysis centers dealing with the broader aspects of the National Measurement System; provides appropriate services to ensure that the NBS staff has optimum accessibility to the scientific information of the world, and directs the public information activities of the Bureau. The Office consists of the following organizational units:

Office of Standard Reference Data—Office of Technical Information and Publications—Library—Office of Public Information—Office of International Relations.

[1] Headquarters and Laboratories at Gaithersburg, Maryland, unless otherwise noted; mailing address Washington, D.C. 20234.
[2] Part of the Center for Radiation Research.
[3] Located at Boulder, Colorado 80302.

U.S. DEPARTMENT OF COMMERCE
Maurice H. Stans, Secretary
NATIONAL BUREAU OF STANDARDS
Lewis M. Branscomb, Director

Order all publications from the Superintendent of Documents
U.S. Government Printing Office, Washington, D.C. 20402

Use of funds for printing this publication approved by the Director of the Bureau of the Budget (June 22, 1966).

a pressure of 101325 Pa (formerly known as 1 standard atmosphere). For gases (symbolized as g), the standard state is that of the ideal gas at a pressure of 101325 Pa. For aqueous solutions (symbolized as aq), the standard state is the hypothetical ideal solution at a concentration of 1 mol kg^{-1} (of solvent); the properties of ideal aqueous ionic solutions are taken equal to the sum of the properties of the individual ions.

The following values of the fundamental constants were employed in the calculations: gas constant, R, (8.31433 ± 0.00120) J $mol^{-1}K^{-1}$; constant relating wave number and energy $(0.1196256 \pm 0.0000107)$ J m mol^{-1}. Relative atomic masses were taken as recommended by the Commission on Atomic Weights of IUPAC (1970). All thermodynamic data in the table relate to the natural mixture of isotopic species. Nuclear spin contributions were ignored. The uncertainties in the table represent the Task Group's estimates of the overall uncertainties at a 95 percent confidence level.

Tentative Set of Key Values for Thermodynamics—Part I

Substance	State	$\Delta H^\circ_{f,298.15}$ kJ mol^{-1}	Footnote	$S^\circ_{298.15}$ J mol^{-1} K^{-1}	$H^\circ_{298.15}-H^\circ_0$ kJ mol^{-1}	Footnote
O	g	249.17 ±0.10	c	160.946±0.020	6.728±0.003	b
O_2	g	0	a	205.037±0.033	8.682±0.004	b
H	g	217.997±0.006†	d	114.604±0.015	6.197±0.002	b
H^+	aq	0	a	0	–	a
H_2	g	0	a	130.570±0.033	8.468±0.003	b
H_2O	l	−285.830±0.042	e	69.950±0.080	–	f
H_2O	g	−241.814±0.042	g	188.724±0.040	9.908±0.008	b
He	g	0	a	126.039±0.012	6.197±0.002	b
Ne	g	0	a	146.214±0.016	6.197±0.002	b
Ar	g	0	a	154.732±0.020	6.197±0.002	b
Kr	g	0	a	163.971±0.020	6.197±0.002	b
Xe	g	0	a	169.573±0.020	6.197±0.002	b
Cl	g	121.290±0.008	h	165.076±0.020	6.272±0.003	b
Cl^-	aq	−167.08 ±0.14	i	56.78 ±0.60	–	i
Cl_2	g	0	a	222.965±0.040	9.180±0.008	b
HCl	g	−92.31 ±0.13	i	186.786±0.033	8.640±0.004	b
Br	g	111.84 ±0.12	j	174.904±0.020	6.197±0.002	b
Br^-	aq	−121.50 ±0.17	k	83.3 ±1.3	–	k
Br_2	l	0	a	152.210±0.040	24.52 ±0.13	l
Br_2	g	30.91 ±0.11	l	245.350±0.054	9.724±0.012	b
HBr	g	−36.38 ±0.17	k	198.585±0.033	8.648±0.004	b
I	g	106.762±0.040	m	180.673±0.020	6.197±0.002	b
I^-	aq	−56.90 ±0.84	n	107.11 ±0.42	–	n
I_2	c	0	a	116.139±0.080	13.196±0.040	o
I_2	g	62.421±0.080	o	260.567±0.063	10.117±0.012	b
HI	g	26.36 ±0.80	n	206.480±0.040	8.657±0.006	b
N	g	472.68 ±0.40	p	153.189±0.020	6.197±0.002	b
N_2	g	0	a	191.502±0.025	8.669±0.003	b
C	c	0	a	5.74 ±0.12	1.050±0.020	q
C	g	716.67 ±0.44	r	157.988±0.020	6.535±0.006	b
CO	g	−110.53 ±0.17	s	197.556±0.032	8.673±0.008	b
CO_2	g	−393.51 ±0.13	t	213.677±0.040	9.364±0.008	b

Tentative Set of Key Values for Thermodynamics—Part I, recalculated to calories*

Substance	State	$\Delta H^\circ_{f,298.15}$ kcal mol^{-1}	$S^\circ_{298.15}$ cal mol^{-1} K^{-1}	$H^\circ_{298.15}-H^\circ_0$ kcal mol^{-1}
O	g	59.553±0.024	38.467±0.005	1.608±0.001
O_2	g	0	49.005±0.008	2.075±0.001
H	g	52.103±0.001†	27.391±0.004	1.481±0.001
H^+	aq	0	0	–
H_2	g	0	31.207±0.008	2.024±0.001
H_2O	l	−68.315±0.010	16.718±0.019	–
H_2O	g	−57.795±0.010	45.106±0.010	2.368±0.002

JOURNAL OF RESEARCH of the National Bureau of Standards—A. Physics and Chemistry
Vol. 75A, No. 2, March–April 1971

Tentative Set of Key Values for Thermodynamics—Part I. Report of the ICSU–CODATA Task Group on Key Values for Thermodynamics, October, 1970*

S. Sunner**

(December 9, 1970)

This paper is a preliminary report from the Task Group on Key Values for Thermodynamics of the Committee on Data for Science and Technology (CODATA) of the International Council of Scientific Unions (ICSU). It gives values agreed upon by the Committee for enthalpies of formation and entropies of 32 atoms, molecules, and ionic species. Sources of the data are also tabulated.

Key words: CODATA; key values; thermodynamics.

EDITOR'S NOTE: In line with the Bureau's role in support of international scientific collaboration efforts of the International Council of Scientific Unions (ICSU), the Journal of Research is publishing this preliminary report on Key Values for Thermodynamics, as prepared by a Task Group of the Committee on Data for Science and Technology (CODATA). It is hoped that the widespread distribution of this report will provide an opportunity for all interested scientists to comment on the proposed values and thus aid the members of the Task Group in their final evaluations. The members of the Task Group are: S. Sunner (Sweden), Chairman, J. D. Cox (U.K.), L. V. Gurvich (U.S.S.R.), D. M. Newitt (U.K.), D. D. Wagman (U.S.A.); consultants to the Group are: C. B. Alcock (Canada), W. H. Evans (U.S.A.), V. A. Medvedev (U.S.S.R.), and I. Wadsö (Sweden). This report has appeared as CODATA Bulletin No. 2, November, 1970.

In 1968, the Committee on Data for Science and Technology (CODATA) of the International Council of Scientific Unions (ICSU) appointed a Task Group on Key Values for Thermodynamics. The first objective of the Task Group is to prepare an internationally agreed set of values of the basic thermodynamic properties of a number of chemical species, including the elements in both standard and monatomic gaseous states, aqueous ions, and simple compounds.

The table below contains the Task Group's first set of proposed values for the standard enthalpies of formation at 298.15 K, $\Delta H^\circ_{f,\,298.15}$, the standard entropies at 298.15 K, $S^\circ_{298.15}$, and the standard enthalpy increments between 0 K and 298.15 K, $H^\circ_{298.15} - H^\circ_0$, of 32 species. The values are based on selections and calculations made at the National Bureau of Standards, U.S.A., and the Institute for High Temperatures of the Academy of Sciences of U.S.S.R., and agreed by the whole Task Group.

By this announcement, the Task Group invites comments from thermodynamicists on the aptness of the proposed values. Any such comments will be gladly received by the Chairman of the Task Group, and will help in the formulation of a first set of recommended key values, to be published in approximately one year's time. Until then, any author who wishes to cite a value from the table below is requested to make clear that the value he cites is tentative. It should be carefully noted that the values now proposed are not fully consistent with the values in any previously published thermodynamic tables, for example the "Technical Notes 270" of the National Bureau of Standards or "Termicheskie Konstanty Weshchesty" of the Academy of Sciences of U.S.S.R. The achievement of consistency between the various thermodynamic tables is of course a long-term objective which the Task Group hopes to facilitate, but for some time to come, inconsistency between the Task Group's recommended values and values already tabulated in other series is inevitable.

The second set of species planned for consideration by the Task Group in the immediate future is likely to include the following: S(g), S(rh), SO_2(g), SO_4^{2-}(aq), NH_3(g), NH_4^+(aq), NO_3^-(aq), OH^-(aq), Na(g), Na(c), Na^+(aq), K(g), K(c), K^+(aq), Li(g), Li(c), Li^+(aq), Rb(g), Rb(c), Rb^+(aq), Cs(g), Cs(c), Cs^+(aq), F(g), F_2(g), HF(g), F^-(aq).

It would assist the Task Group if researchers who have completed measurements that are relevant to the Task Group's work on the second set of species would communicate their results to the Chairman of the Task Group in advance of publication.

In the table below, the usual definitions of standard states have been adopted. For crystalline solids (symbolized as c) and for liquids (symbolized as l), the standard state is that of the pure substance under

*An invited paper.

**Chairman, CODATA Task Group on Key Values for Thermodynamics. Thermochemistry Laboratory, Lund University, POB 740, S–220 07, Lund 7, Sweden.

Tentative Set of Key Values for Thermodynamics—Part I, recalculated to calories*—continued

Substance	State	$\Delta H°_{f,298.15}$ kcal mol^{-1}	$S°_{298.15}$ cal mol^{-1} K^{-1}	$H°_{298.15}-H°$ kcal mol^{-1}
He	g	0	30.124 ± 0.003	1.481 ± 0.001
Ne	g	0	34.946 ± 0.004	1.481 ± 0.001
Ar	g	0	36.982 ± 0.005	1.481 ± 0.001
Kr	g	0	39.190 ± 0.005	1.481 ± 0.001
Xe	g	0	40.529 ± 0.005	1.481 ± 0.001
Cl	g	28.989 ± 0.002	39.454 ± 0.005	1.499 ± 0.001
Cl^-	aq	−39.933 ± 0.033	13.57 ± 0.14	–
Cl_2	g	0	53.290 ± 0.010	2.194 ± 0.002
HCl	g	−22.063 ± 0.031	44.643 ± 0.008	2.065 ± 0.001
Br	g	26.730 ± 0.029	41.803 ± 0.005	1.481 ± 0.001
Br^-	aq	−29.039 ± 0.041	19.91 ± 0.31	–
Br_2	†	0	36.379 ± 0.010	5.860 ± 0.031
Br_2	g	7.388 ± 0.026	58.640 ± 0.013	2.324 ± 0.003
HBr	g	−8.695 ± 0.041	47.463 ± 0.008	2.067 ± 0.001
I	g	25.517 ± 0.010	43.182 ± 0.005	1.481 ± 0.001
I^-	aq	−13.60 ± 0.20	25.60 ± 0.10	–
I_2	c	0	27.758 ± 0.019	3.154 ± 0.010
I_2	g	14.919 ± 0.019	62.277 ± 0.015	2.418 ± 0.003
HI	g	6.30 ± 0.19	49.350 ± 0.010	2.069 ± 0.002
N	g	112.97 ± 0.10	36.613 ± 0.005	1.481 ± 0.001
N_2	g	0	45.770 ± 0.006	2.072 ± 0.001
C	c	0	1.372 ± 0.029	0.251 ± 0.005
C	g	171.29 ± 0.11	37.760 ± 0.005	1.562 ± 0.002
CO	g	−26.417 ± 0.041	47.217 ± 0.008	2.073 ± 0.002
CO_2	g	−94.051 ± 0.031	51.070 ± 0.010	2.238 ± 0.002

†Due to a calculation error these data were given in the original report as 218.002 kJ mol^{-1} (52.104 kcal mol^{-1}).
*cal = 4.184 *J*.

Footnotes

a. Defined reference state.

b. Calculated, by direct summation over the energy levels, at the Institute for High Temperatures (U.S.S.R.) and the National Bureau Standards (U.S.A.). The uncertainty given includes a contribution of 0.015% of the entropy due to the uncertainty in *R*.

c. Calculated using $D_0(O_2) = 41260 \pm 15$ cm^{-1} from Brix and Herzberg (1954), assuming the products are O atoms in the ground state.

d. Calculated using $D_0(H_2) = 36118.3 \pm 1$ cm^{-1} from Herzberg (1970).

e. Enthalpy of formation of H_2O (l) from Rossini (1931, 1939), and King and Armstrong (1968).

f. Calculated from $S°_{298.15}$ H_2O(g) with appropriate data for the entropies of expansion to saturation, correction to the real vapour and vaporization, from Keenan, Keyes, Hill, and Moore (1969). See also Giauque and Stout (1936).

g. Calculated from $\Delta H°_{f,298.15}$ H_2O(l) using data from Keenan, Keyes, Hill, and Moore (1969).

h. Calculated using $D_0(Cl_2) = 19997 \pm 1$ cm^{-1} based on Douglas, Møller, and Stoicheff (1963), LeRoy and Bernstein (1970), LeRoy (1970), and Sitterly (1970).

i. Enthalpy of formation of HCl(g) from Rossini (1932), Roth and Richter (1934), von Wartenberg and Hanisch (1932), Lacher, Kianpour, Oetting, and Park (1956), Faita, Longhi, and Mussini (1967), Cerquetti, Longhi, and Mussini (1968), and King and Armstrong (1970). Enthalpy of solution of HCl(g) from Gunn and Green (1963), Gunn (1964), Vanderzee and Nutter (1963), and Roth and Bertram (1937). Gibbs energy of solution from Bates and Kirschman (1919), Haase, Naas, and Thumm (1963), and Aston and Gittler (1955). Entropy of Cl^-(aq) from Bates and Bower (1954), and Greeley, Smith, Stoughton, and Lietzke (1960), on the Ag, AgCl, Cl^- electrode. See also Cerquetti, Longhi, and Mussini (1968).

j. Calculated using $D_0(^{79}Br\ ^{81}Br) = 15893.1 \pm 2$ cm^{-1} based on Horsley and Barrow (1967), and Sitterly (1970). LeRoy (1970) recalculated $D_0(Br_2)$ from these data; his result is correct only if Horsley and Barrow missed many upper rotational levels of higher vibrational states in their interpretation of the absorption spectra.

k. Enthalpy of formation from Johnson and Sunner (1963), Johnson and Ambrose (1963), Sunner and Thorén (1964), Lacher, Casali, and

Park (1956), and Howard and Skinner (1966). Enthalpy of solution of HBr(g) from Vanderzee and Nutter (1963), Roth and Bertram (1937), and Thomsen (1884). The entropy of Br^-(aq) from measurements on the Ag, AgBr, Br^- electrode by Hetzer, Robinson, and Bates (1962), Harned, Keston, and Donelson (1936), and Own and Foering (1936), and from differences in the entropy of solution for the salt pairs KCl-KBr, CsCl-CsBr, AgCl-AgBr, and NaCl-NaBr.$2H_2O$.

l. From the specific heat and heat of vaporization measurements of Hildenbrand et al. (1958).

m. Calculated using $D_0(I_2) = 12440.9 \pm 1.1$ cm^{-1} from LeRoy (1970), Brown (1931), LeRoy and Bernstein (1970), and Sitterly (1970).

n. Enthalpy of formation of I^-(aq) from Vorob'ev, Broier and Skuratov (1966), Wu, Birkey, and Hepler (1963), and Howard and Skinner (1966). Entropy of I^-(aq) from measurements on the Ag, AgI, I^- electrode by Hetzer, Robinson, and Bates (1964), Kortüm and Häussermann (1965), and Feakins and Watson (1963), and from differences in the entropy of solution for the salt pairs KCl-KI, CsCl-CsI, AgCl-AgI, and NaCl-NaI.$2H_2O$. Enthalpy of formation of HI(g) from Taylor and Crist (1941), Rittenberg and Urey (1934), Bright and Hagerty (1947), Murphy (1936), and Günther and Wekua (1931).

o. From the low-temperature specific heat data of Shirley and Giauque (1959), and vapour pressure data of Baxter, Hickey, and Holmes (1907), Baxter and Grose (1915), Gillespie and Fraser (1936), and Stern (1958).

p. Calculated from $D_0(N_2) = 78715 \pm 50$ cm^{-1} from Buttenbender and Herzberg (1935), Tanaka, Ogawa, and Jursa (1964), Tilford, Vanderslice and Wilkinson (1965), and Sitterly (1970). See the discussion in Gaydon (1968).

q. Graphite is selected as the standard reference state for carbon. However, there is considerable variation in the measured values of the low-temperature heat capacity and entropy, depending upon the source and nature of the graphite sample. See DeSorbo (1955), DeSorbo and Nichols (1958), DeSorbo and Tyler (1953). We have used the measurements of DeSorbo and Tyler on Acheson spectroscopic graphite, corresponding to the material used for the determination of the heat of formation of CO_2(g).

r. Calculated using $D_0(CO) = 89595 \pm 30$ cm^{-1} from Douglas and Møller (1955), assuming the products are $C(^3P_0)$ and $O(^3P_2)$.

s. Heat of formation of CO(g) from combustion measurements of Rossini (1931, 1939), Awbery and Griffiths (1933), and Fenning and Cotton (1933), and equilibrium measurements by Smith (1946), Neumann and Köhler (1928), Peters and Mobius (1958), and Meyer and Scheffer (1938).

t. Heat of formation from Prosen and Rossini (1944), Hawtin, Lewis, Moul, and Phillips (1966), Dewey and Harper (1938), Jessup (1938), and Lewis, Frisch, and Margrave (1965). Much of the uncertainty relates to the difference in the various samples of graphite that have been studied.

Bibliography

Aston, J. G.; Gittler, F. L., J. Am. Chem. Soc. **77**, 3173 (1955).
Awbery, J. H.; Griffiths, E., Proc. Roy. Soc. (London) **A141**, 1 (1933).
Bates, S. J.; Kirschman, H. D., J. Am. Chem. Soc. **41**, 1991 (1919).
Bates, R. G.; Bower, V. E., J. Res. Nat. Bur. Stand. (U.S.), **53**, 283 (1954).
Baxter, G. P.; Grose, M. R., J. Am. Chem. Soc. **37**, 1061 (1915).
Baxter, G. P.; Hickey, C. H.; Holmes, W. C., J. Am. Chem. Soc. **29**, 127 (1907).
Bright, N. F. H.; Hagerty, R. P., Trans. Faraday Soc. **43**, 697 (1947).
Brix, P.; Herzberg, G., Can. J. Phys. **32**, 110 (1954).
Brown, W. G., Phys. Rev. **38**, 709 (1931).
Buttenbender, G.; Herzberg, G., Ann. Physik [5], **21**, 577 (1935).
Cerquetti, A.; Longhi, P.; Mussini, T., J. Chem. Eng. Data **13**, 458 (1968).
Commission on Atomic Weights of IUPAC, Pure Appl. Chem. 1970, **21**, 95 (1970).
DeSorbo, W., J. Chem. Phys. **23**, 1970 (1955); J. Am. Chem. Soc. **77**, 4713 (1955).
DeSorbo, W.; Nichols, G. F., J. Phys. Chem. Solids **6**, 352 (1958).
DeSorbo, W.; Tyler, W. W., J. Chem. Phys. **21**, 1660 (1953).
Dewey, P. H.; Harper, D. R., J. Res. Nat. Bur. Stand. (U.S.), **21**, 457 (1938).
Douglas, A. E.; Møller, C. K., Can. J. Phys. **33**, 125 (1955).
Douglas, A. E.; Møller, C. K.; Stoicheff, B. P. Can. J. Phys. **41**, 1174 (1963).
Faita, G.; Longhi, P.; Mussini, T., J. Electrochem. Soc. **114**, 340 (1967).
Feakins, D.; Watson, P., J. Chem. Soc. 4686 (1963).
Fenning, R. W.; Cotton, F. T., Proc. Roy. Soc. (London) **A141**, 17 (1933).
Gaydon, A. G., Dissociation Energies and Spectra of Diatomic Molecules (3d Ed. Chapman and Hall, London, 1968).
Giauque, W. F.; Stout, J. W., J. Am. Chem. Soc. **58**, 1144 (1936).
Gillespie, L. J.; Fraser, L. H. D., J. Am. Chem. Soc. **58**, 2260 (1936).
Greeley, R. S.; Smith, W. T.; Stoughton, R. W.; Lietzke, M. H., J. Phys. Chem. **64**, 652 (1960).
Gunn, S. R., U.S. Atomic Energy Comm. Rept. UCRL 7992 (1964).
Gunn, S. R.; Green, L. G., J. Chem. Eng. Data **8**, 180 (1963).
Günther, P.; Wekua, K., Z. Physik. Chem. **A154**, 193 (1931).
Haase, R.; Naas, H.; Thumm, H., Z. Physik. Chem. (Frankfurt) (N. F.) **37**, 210 (1963).
Harned, H. S.; Keston, A. S.; Donelson, J. G., J. Am. Chem. Soc. **58**, 989 (1936).
Hawtin, P.; Lewis, J. B.; Moul, N.; Phillips, R. H., Trans. Roy. Soc. (London) **A261**, 67 (1966).
Herzberg, G., J. Mol. Spectroscopy **33**, 147 (1970).
Hetzer, H. B.; Robinson, R. A.; Bates, R. G., J. Phys. Chem. **66**, 1423 (1962).
Hetzer, H. B.; Robinson, R. A.; Bates, R. G., J. Phys. Chem. **68**, 1929 (1964).
Hildenbrand, D. L.; Kramer, W. R.; McDonald, R. A.; Stull, D. R., J. Am. Chem. Soc. **80**, 4129 (1958).
Horsley, T. A.; Barrow, R. F., Trans. Faraday Soc. **63**, 32 (1967).
Howard, P. B.; Skinner, H. A., J. Chem. Soc. 1536 (1966).
Jessup, R. S., J. Res. Nat. Bur. Stand. (U.S.), **21**, 475 (1938).
Johnson, W. H.; Ambrose, J. R., J. Res. Nat. Bur. Stand. (U.S.), **67A** (Phys. and Chem), 427 (1963).
Johnson, W. H.; Sunner, S., Acta Chem. Scand. **17**, 1917 (1963).
Keenan, J. H.; Keyes, F. G.; Hill, P. G.; Moore, J. G., Steam Tables (John Wiley & Sons, Inc., New York, 1969).
King, R. Armstrong, G. T., J. Res. Nat. Bur. Stand. (U.S.), **72A**, (Phys. and Chem.), No. 2, 113 (1968).
King, R.; Armstrong, G. T., J. Res. Nat. Bur. Stand. (U.S.), **74A** (Phys. and Chem.), No. 6, **769** (1970).
Kortüm, G.; Häussermann, W. F., Ber. Bunsenges. Physik. Chem. **69**, 594 (1965).
Lacher, J. R.; Casali, L.; Park, J. D., J. Phys. Chem. **60**, 607 (1956).
Lacher, J. R.; Kianpour, A.; Oetting, F.; Park, J. D., Trans. Faraday Soc. **52**, 1500 (1956).
LeRoy, R. T., Chem. Phys. Letters **5**, 42 (1970).
LeRoy, R. T.; Bernstein, R. B., J. Chem. Phys. **52**, 2678, 3869 (1970).
Lewis, D. C.; Frisch, M. A.; Margrave, J. L., Carbon **2**, 431 (1965).
Meyer, G.; Scheffer, F. E. C., Rec. trav. chim. **57**, 604 (1938).
Murphy, G. M., J. Chem. Phys. **4**, 344 (1936).
Neumann, B.; Köhler, G., Z. Elektrochem. **34**, 218 (1928).

Owen, B. B.; Foering, L., J. Am. Chem. Soc. **58**, 1575 (1936).
Peters, H.; Mobius, H. H., Z. Physik. Chem. **209**, 298 (1958).
Prosen, E. J.; Rossini, F. D., J. Res. Nat. Bur. Stand. (U.S.), **33**, 439 (1944).
Rittenberg, D.; Urey, H. C., J. Chem. Phys. **2**, 106 (1934).
Rossini, F. D., J. Res. Nat. Bur. Stand. (U.S.), **6**, 1 and 36 (1931).
Rossini, F. D., J. Res. Nat. Bur. Stand. (U.S.), **9**, 679 (1932).
Rossini, F. D., J. Res. Nat. Bur. Stand. (U.S.), **22**, 407 (1939).
Roth, W. A.; Bertram, A., Z. Elektrochem. **43**, 376 (1937).
Roth, W. A.; Richter, H., Z. Physik. Chem. **A170**, 123 (1934).
Shirley, D. A.; Giauque, W. F., J. Am. Chem. Soc. **81**, 4778 (1959).
Sitterly, C. M., Nat. Bur. Stand. (U.S.), Washington, D.C. (Private commun.).
Smith, R. P., J. Am. Chem. Soc. **68**, 1163 (1946).
Stern, T. H., Ph. D. Thesis, Univ. of Washington (1958).
Sunner, S.; Thorén, S., Acta Chem. Scand. **18**, 1328 (1964).
Tanaka, Y.; Ogawa, M.; Jursa, A. S., J. Chem. Phys. **40**, 3690 (1964).
Taylor, A. H.; Crist, K. H., J. Am. Chem. Soc. **63**, 1377 (1941)
Thomsen, J., Thermochemische Untersuchungen (J. Barth, Leipzig, 1884).
Tilford, S. G.; Vanderslice, J. T.; Wilkinson, P. G., Astrophys. J. **142**, 1203 (1965).
Vanderzee, C. E.; Nutter, J. D., J. Phys. Chem. **67**, 2521 (1963).
Vorob'ev, A. F.; Broier, A. F.; Skuratov, S. M., Dokl. Akad. Nauk SSSR **173**, 385 (1966).
von Wartenberg, H.; Hanisch, K., Z. Physik. Chem. **A161**, 413 (1932).
Wu, C.; Birkey, M. M.; Hepler, L. G., J. Phys. Chem. **67**, 1202 (1963).

(Paper 75A2–651)

JOURNAL OF RESEARCH of the National Bureau of Standards – A. Physics and Chemistry
Vol. 75A, No. 2, March–April 1971

Expanded Formulation of Thermodynamic Scaling in the Critical Region

Martin J. Cooper

Institute for Basic Standards, National Bureau of Standards, Washington, D.C. 20234

(December 18, 1970)

A description of the thermodynamic properties in the critical region of a physical system is obtained from a scaled expression for the free-energy $F(\rho, T)$. In general, a nonsymmetric coexistence curve is predicted, with the symmetric case (e.g., magnets) included as a special example. For fluids, deviations from symmetry give rise to an expression for the average density below the critical point nonlinear in the temperature near T_c (in contrast to the usual "law of rectilinear diameter"); these asymmetries also contribute to the discontinuity in the specific heat along the critical isochore. To lowest order, the formulation reduces to Widom's homogeneous scaling; the classical equations of state of the van der Waals type are incorporated as a special case.

Key words: Critical region; equation of state; liquid-gas transition; phase boundary; phase transition; thermodynamic scaling.

1. Introduction

The Widom-Kadanoff-Domb scaling hypothesis [1–3][1] provides a qualitative characterization for the thermodynamic features of a second-order phase transition [4]. Scaling incorporates the usual power law forms for the various physical anomalies and more generally serves as a lowest order asymptotic description close to the critical point [5]. Such limiting behavior has been found in various mathematical models and also appears to be valid in real systems.

Despite the relative success of the scaling approach, there remains a definite need for a more global picture of the critical region. This is evident during the analysis of bulk thermodynamic data where there exists first the problem of determining those physical quantities which satisfy the basic conditions required by simple scaling. For some systems, this selection is easily based upon some known/intrinsic physical property (symmetry); whereas for others, the actual choice is less certain [5]. The determination is further complicated by the secondary problem, that of estimating the actual range over which scaling remains valid [6].

These difficulties are particularly evident in the application of the scaling description to real fluids near their critical point [4]. Here there is some experimental indication of a partial anti-symmetry about the critical isochore in the chemical potential μ – number density ρ representation not present with either the pressure p or the specific volume v coordinates. It is also known, however, that the phase boundary lacks this same symmetry in any set of variables. The coexistence curve is rather asymmetric about the critical isochore with such deviations being described by the empirical "law of rectilinear diameter." Despite the fact that this nonsymmetric behavior cannot be accommodated within the usual lowest order scaling description, the fluid data appear to scale in the preferred μ-ρ coordinates over a rather large region about the critical point (in a density range of ± 30 percent and a temperature width of several percent from their reduced critical values [4]).

An understanding and resolution of such behavior is hampered by an almost complete ignorance of what is beyond the lowest order scaling description. Since any results will be biased by the neglect of unknown terms, one cannot hope to extract any more than a simple qualitative picture from the experimental data without some knowledge as to the structure of corrections to the asymptotic scaling form. The present article represents an attempt to gain some insight into the structure of such terms. The idea was to construct a "model" calculation incorporating modification of the usual scaling formulation. Based upon an extension of classical thermodynamic ideas, the scheme describes systems lacking any known or simple symmetry and extends a scaling interpretation over an enlarged region about the transition. The approach allows for the first time discussion of the various contributions arising from asymmetry and higher ordered corrections to the asymptotic scaling behavior and their influence on observable physical properties. (After completing the

[1] Figures in brackets indicate the literature references at the end of this paper.

work reported here, we learned that Domb and Gaunt have looked at the structure of correction terms to the completely symmetric Ising model equation of state [7].)

It should be pointed out, however, that the formulation given here is just one possible way of going beyond simple asymptotic scaling. For this reason, it is most important to emphasize the underlying formal structure rather than any of the individual numerical results. While the discussion is applied to fluid systems, the approach is easily adopted to other physical situations. The magnetic problem, with a completely symmetric phase boundary, has been discussed elsewhere [8].

2. Formulation

Our approach is based upon two relatively simple observations. Just as in Widom's original hypothesis [1], classical thermodynamics suggests the framework of our analysis. First, recall that from a free-energy function analytic in two physical variables, density ρ and temperature T, one will obtain an equation of state exhibiting in general a nonsymmetric phase boundary, deviations from a completely symmetric coexistence curve giving rise to a finite slope of the rectilinear diameter. With such behavior, however, one also acquires the classical (van der Waals-like) and quite incorrect description of the critical region [9]. Thus, instead of using such physical variables, we shall follow Widom [1] and assume the thermodynamic properties near the critical point are appropriately described in terms of one intensive physical quantity and one suitably reduced variable x. Moreover, the description is to be consistent with the homogeneity hypothesis, i.e., all functions are to be regular and of a general homogeneous form [5]. The existence of such nonclassical forms has been demonstrated in various model calculations where the scaling behavior appears as the first term in an expansion about the critical point. As an example, Cooper and Green [10] found that the appropriate free-energy of the Bose fluid is a function of the reduced temperature $t=(T-T_c)/T_c$ and a reduced variable $x=t\,|\,\Delta\rho\,|^{-1/\beta}$, $\Delta\rho=(\rho-\rho_c)/\rho_c$ with the scaling form as the dominant term in an expansion containing higher ordered homogeneous terms. (Gaunt and Domb [7] have suggested a similar structure which applies to the Ising model.) As our second point, we shall assert that in general the free-energy density in the critical region is given by a convergent expansion of the form

$$F(\rho, T)-F_0(\rho, T)=|\,\Delta\rho\,|^{\delta+1}\sum_{s=1}^{\infty}(\Delta\rho)^{s-1}f_s(x) \tag{1}$$

where $x=t\,|\,\Delta\rho\,|^{-1/\beta}$. Here both $1/\beta$ and δ are to be arbitrary constants (not necessarily integer) and $F_0(\rho, T)$ denotes any smooth analytic part of the free-energy near the transition ρ_c, T_c. It is implicitly assumed that the function $F(\rho, T)$ is single value everywhere and satisfies the well-known convexity conditions for thermodynamic stability [5]. The set of functions $\{f_s(x)\}$ are to be "well behaved" in the variable $x=t\,|\,\Delta\rho\,|^{-1/\beta}$ over the real interval of interest (min $x_0^+)\leqslant x\leqslant+\infty$. (We require only that $F(\rho, T)$ satisfy the physical conditions of continuity and differentiability in the single-phase region with each $f_s(x)$ analytic for x less than some finite constant R (see below).) Equivalently, one could take similar expressions for the chemical potential $\mu(\rho, T)$ and the pressure $p(\rho, T)$ about the critical point $\rho=\rho_c$, $t=0$:

$$\mu(\rho, T)=\mu_c+\mu_0(t)+|\,\Delta\rho\,|^{\delta-1}\sum_{s=1}^{\infty}(\Delta\rho)^s\mu_s(x), \tag{2}$$

$$p(\rho, T)=p_c+p_0(t)+|\,\Delta\rho\,|^{\delta-1}\sum_{s=1}^{\infty}(\Delta\rho)^s p_s(x). \tag{3}$$

Both thermodynamic forces are to be well-behaved everywhere in the single-phase region and also on the phase boundary (except perhaps at the critical point). These expressions are also consistent with the experimental observation that both p and μ have continuous first derivatives across the critical isochore. The dominant $s=1$ term of these expansions represent the usual asymptotic scaling expressions. The functions $\mu_s(x)$ and $p_s(x)$ are not independent but are themselves related to the set $\{f_s(x)\}$ through the thermodynamic relations

$$p(\rho, T)=\rho^2\left.\frac{\partial F(\rho, T)}{\partial\rho}\right|_T \tag{4}$$

and

$$\mu(\rho, T)=\left(1+\rho\frac{\partial}{\partial\rho}\right)_T F(\rho, T). \tag{5}$$

The form of $F_0(\rho, T)$ must be consistent with the expressions for μ and p. The first few important relations of this hierarchy are that

$$\left[\delta+1-\frac{x}{\beta}\frac{\partial}{\partial x}\right]f_1(x)=\mu_1(x)=\rho_c^{-1}p_1(x) \tag{6}$$

and

$$\rho_c^{-1}p_2(x)-\mu_2(x)=\left[\delta-\frac{x}{\beta}\frac{\partial}{\partial x}\right]f_1(x). \tag{7}$$

2.1. Two-Phase Region

Below the critical temperature, $t<0$, we seek simultaneous (non-trivial) solutions to the conditions for thermodynamic stability of coexisting phases, ρ_L and ρ_G,

$$p(\rho_L, T)=p(\rho_G, T)\text{ and }\mu(\rho_L, T)=\mu(\rho_G, T). \tag{8}$$

Denoting the two branches by $\rho_L-\rho_c=\Delta\rho^+$ and $\rho_G-\rho_c=\Delta\rho^-$, with $\Delta\rho^{\pm}=\pm(|t|/|x^{\pm}|)^{\beta}$, the shape of the phase boundary is found by expanding eqs (2) and (3) in a Taylor series about $x_0^{\pm}$ respectively, algebraic consistency requiring that

$$x^{\pm}=x_0^{\pm}+x_1^{\pm}|t|^{\beta}+x_2^{\pm}|t|^{2\beta}+\ldots. \tag{9}$$

Matching the various powers in $|t|^{\beta}$ we find that

(i) $x_0^+ = x_0^- = -x_0$, with both $\mu_1(x)$ and $p_1(x)$ vanishing at $x = -x_0$;

(ii) $x_1^+ = -x_1^- = x_1$ where $x_1 = |-x_0|^{1-\beta}$

$$\cdot \left[\frac{p_3(x) - \rho_c \mu_3(x)}{\left(\beta(\delta+1) - x \frac{\partial}{\partial x} \right)(p_2(x) - \rho_c \mu_2(x))} \right]_{x=-x_0};$$

(iii) in general $x_r^+ = (-1)^r x_r^- = x_r$.

Thus we identify $\mu_1(x)$ with Griffith's [5] $h(x)$ function and the condition that $h(x = -x_0)$ vanish along the phase boundary.

With the boundary condition $\mu_1(-x_0) = 0$ we can also solve the differential equation (6) for $f_1(x)$. The homogeneous solution is a constant times $|x|^{\beta(\delta+1)}$; the general solution may be written as

$$f_1(x) = x^{\beta(\delta+1)} \left[\frac{f_1(-x_0)}{|-x_0|^{\beta(\delta+1)}} - \beta \int_{-x_0}^{x} dy \, \frac{\mu_1(y)}{y^{\beta(\delta+1)}} \right]. \quad (10)$$

The difference between the two coexisting densities is found to be given by

$$\rho_L - \rho_G = \left[\frac{2}{|-x_0|^{\beta}} \right] |t|^{\beta} + \left[\frac{\beta(\beta+1)}{2} \left(\frac{x_1}{x_0} \right)^2 + \frac{x_2}{x_0} \right] |t|^{3\beta} + \ldots \quad (11)$$

Deviations from a completely symmetric coexistence curve are described by the mean density of the two phases

$$\bar{\rho} = \frac{1}{2}(\rho_L + \rho_G) = \rho_c + \left[\frac{-\beta x_1}{|-x_0|^{\beta+1}} \right] |t|^{2\beta} + O(|t|^{4\beta}). \quad (12)$$

This is equivalent to the usual "law of rectilinear diameter" in the classical case ($\beta = 1/2$), but has the curious feature that for real fluids ($\beta < 1/2$) the average density ρ is curved and comes into the critical point with zero slope. See figure 1. When $x_1 = 0$, the phase boundary is symmetric to this order.

It is also possible to describe the form of the vapor pressure curve using the equation for $p(\rho, T)$

$$p_{\text{coex.}}(\rho, T) = p_c + p_0(t) + |t|^{\beta(\delta+1)} \left[\frac{p_2(-x_0)}{|-x_0|^{\beta(\delta+1)}} + O(t^{2\beta}) \right] \quad (13)$$

with a similar expression for the chemical potential in the two-phase region (replace p_s by μ_s). Here $p_0(t)$ is a smooth analytic function in the temperature.

While the specific heat C_v in the two-phase region can be obtained from the free-energy $F(\rho, T)$, it is perhaps more interesting to look at the individual contributions from the chemical potential μ and pressure p as exhibited in the thermodynamic identity (Yang and Yang [11])

$$\rho C_v = T \left(\frac{\partial^2 p}{\partial T^2} \right)_{\rho} - \rho T \left(\frac{\partial^2 \mu}{\partial T^2} \right)_{\rho}. \quad (14)$$

As the critical point is approached from below T_c along the critical isochore $\rho = \rho_c$, the anomalous temperature variation is given by

$$\frac{\rho_c C_v}{T} = A_- \cdot |t|^{\beta(\delta+1)-2} + O(t^{\beta(\delta+3)-2}) \quad (15)$$

where

$$A_- = \beta(\delta+1)\{\beta(\delta+1) - 1\} \left[\frac{p_2(-x_0) - \rho_c \mu_2(-x_0)}{|-x_0|^{\beta(\delta+1)}} \right].$$

Here the expressions for the pressure (13) and chemical potential on the phase boundary have been used and it has been assumed that the difference $p_2(x) - \rho_c \mu_2(x)$ does not vanish at $x = -x_0$. The asymptotic behavior of the specific heat is thus characterized by a critical exponent $\alpha = 2 - \beta(\delta+1)$ and a coefficient determined entirely by the form of $f_1(x)$ at $x = -x_0$ (see eq (7)). In the simple scaling formulation where $\mu(\rho, T)$ is regular, the divergence of the specific heat along the critical isochore ($T < T_c$) comes entirely from the $(\partial^2 p/\partial T^2)_{\rho_c}$ contribution. This formulation permits contributions from either the pressure and chemical potential by treating both thermodynamic forces on an equal basis.

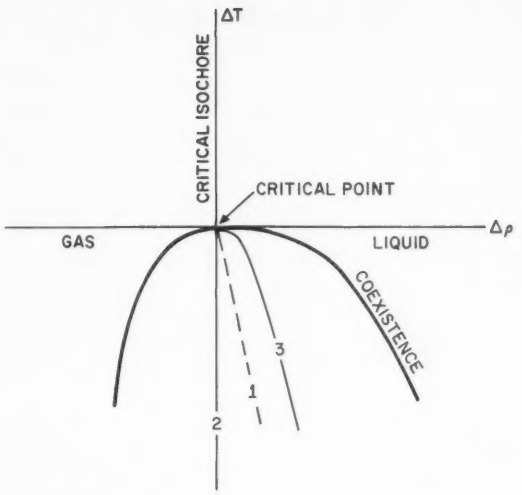

FIGURE 1. *Locus of mean densities for coexisting Phases.*

Curve 1 (dashed line)–usual rectilinear diameter;
Curve 2 (vertical line)–line of mean density of completely symmetric phase boundary like that supposed by lowest order scaling;
Curve 3 (solid line)–locus of mean densities suggested by eq (12).

2.2. Single-Phase Region

All of the thermodynamic properties of the homogeneous fluid in the one-phase region can be obtained directly from the free-energy $F(\rho, T)$. We assume that no higher order discontinuities exist anywhere in this region including the critical isochore $x=\infty$. This implies that the expression for $\mu(\rho, T)$ and $p(\rho, T)$ in the (x, t) plane exist and are everywhere convergent for large $R < x \leq \infty$.

In general, the isothermal compressibility K_T is given by

$$[\rho^2 K_T]^{-1} = \left(\frac{\partial \mu}{\partial \rho_T}\right)$$

$$= \frac{|\Delta\rho|^{\delta-1}}{\rho_c} \sum_{s=1}^{\infty} (\Delta\rho)^{s-1} \left[(\delta+s-1) - \frac{x}{\beta}\frac{\partial}{\partial x} \right] \mu_s(x) \quad (16)$$

with the thermodynamic stability [5] requiring that K_T be everywhere non-negative. The dominant thermodynamic behavior near the critical isochore (x large) is given by the leading term in this expression ($s=1$) and is like that found from simple scaling. As the critical point is approached along the coexistence curve within the single-phase region, the compressibility diverges as $|t|^{-\gamma'}$ where $\gamma' = \beta(\delta-1)$, provided $\mu_1'(-x_0) \neq 0$.

The thermodynamic behavior of the specific heat in the homogeneous phase is given by

$$C_v = -T(\partial^2 F/\partial T^2)\rho,$$

which may be written as

$$C_v = \frac{1+t}{\rho_c T_c} \sum_{s=1}^{\infty} |t|^{\beta(\delta+s-1)-2} \left[\frac{p_s''(x) - \rho_c\{\mu_s''(x) + \mu_{s-1}''(x)\}}{x^{\beta(\delta+s-1)-2}} \right] \quad (17)$$

with $\mu_0(x)=0$ (neglecting the smooth contribution from $F_0(\rho, T)$). Since $p_1(x) = \rho_c \mu_1(x)$, the lowest possible contribution to the specific heat must come from an $s \geq 2$ term in this expression. Here in the single phase, just as in the two-phase region, the available experimental evidence suggests that the pressure term $(\partial^2 p/\partial T^2)\rho_c$ is much larger than the chemical potential term [12]. About the critical isochore above T_c, the specific heat varies as $|t|^{-\alpha}$, where $\alpha = 2-\beta(\delta+\mathbf{s}-1)$, with $\mathbf{s}$ determined by the first nonvanishing term in the limit as $x \to \infty$. (The anomaly in the specific heat along the critical isochore is also given by $F_{\mathbf{r}}\,|t|^{-\alpha}$, where $\alpha = 2-\beta(\delta+\mathbf{r})$ and $F_{\mathbf{r}}$ denotes the limit of $f_{\mathbf{r}}(x) \cdot x^{-\beta(\delta+\mathbf{r}-1)}$ as $x \to \infty$.] Such structure admits the possibility of different values for the critical indices α and α'. If, for example, the leading $\mathbf{s}'=2$ were finite in the two-phase region and then vanish above T_c at large x [see eqs 15, 17], $\mathbf{s}$ would be greater than 2 and thus the difference $|\alpha-\alpha'| = \beta|\mathbf{s}-\mathbf{s}'|$ could be greater than zero.

3. Discussion

The extended formulation of thermodynamic scaling presented here provides a quite general description for the critical region of a fluid. The formalism proceeds beyond the usual lowest order asymptotic behavior and accommodates both the chemical potential and pressure as equivalent physical variables. Within the description it is possible to note contributions from the various higher ordered terms ($s > 1$) and of the two quantities p, μ to the various physical anomalies. We found, for example, that the difference between the potential and pressure variables is not only reflected in the shape of the coexistence curve (as determined by the value of x_1), but also enters into the leading behavior of the specific heat.

We also expect extended scaling to be valid beyond the asymptotically small range of simple scaling, with contributions from the additional terms affecting the determination of the values of the critical indices away from the acutal critical point. For example, the experimentally determined shape of the coexistence curve β^* would be greater or less than the true β, the modification depending upon both the sign and magnitude of the additional terms of eq (1).

In the rather special cases where $1/\beta$ is an even integer, the formulation recovers the classical thermodynamic description of a van der Waals system. For $\beta = 1/2$, this is just the familiar parabolic coexistence curve of the mean-field result, with the usual rectilinear diameter $\bar{\rho} = \rho_c + \rho_2|t|$.

As mentioned before, any comparison of these results to the physical features must remain somewhat qualitative. This is because the formulation is essentially analytic everywhere and must therefore suffer the same defects as all "classical" equations of state. However, we believe the utility of this analysis lies in the display of certain features which must eventually be contained in any complete thermodynamic description of the critical region.

The author wishes to thank J. M. H. Levelt-Sengers and Melville S. Green for discussions involving this work.

4. References

[1] Widom, B., J. Chem. Phys. **43,** 3898 (1965).
[2] Kadanoff, L., et. al., Rev. Mod. Phys. **39,** 395 (1967). See also Fisher, M. E., Repts. Prog. Phys. **XXX,** 615 (1967).
[3] Domb, C., and Hunter, D. L., Proc. Phys. Soc. **86,** 1147 (1965). Compare their series in the Ising model to our eq 2.
[4] Vicentini-Missoni, Levelt Sengers, J. H. M., and Green, M. S., J. Res. Nat. Bur. Stand. (U.S.), **73A** (Phys. and Chem.), 563 (1969); also Phys. Rev. Letters **18,** 1113 (1967).
[5] A complete discussion of the thermodynamic properties of simple scaling is given by Griffiths, R. B., Phys. Rev. **158,** 176 (1967).

[6] From a three-dimensional Ising calculation, D. Gaunt and C. Domb (J. Phys. London **2,** C-1038 (1968)) estimate that true asymptotic critical behavior is evident only for $t=1-T/T_c<10^{-4}$. The data for He^4, CO_2, Xe in ref. [4], seem to scale over a density range of ± 30 percent and a temperature width of several percent about the critical point.
[7] Domb, C., and Gaunt, D. S., IUPAP International Magnetism Conference, Grenoble (1970).
[8] Cooper, M. J., IUPAP International Magnetism Conference, Grenoble (1970).
[9] van Laar, J., Comm. Kon. Akad. Amsterdam **14,** 1091 (1911-12); Baehr, H. D., B.W.K. **15,** 514 (1963). Also Levelt Sengers, J. M. H., paper 51f of A.I.Ch.E., Washington, 1969.
[10] Cooper, M. J., and Green, M.S., Phys. Rev. **176,** 302 (1968).
[11] Yang, C. N., and Yang, C. P., Phys. Rev. Letters **13,** 303 (1964).
[12] From discussion of the apparent antisymmetry of real fluids in ref. [4].

(Paper 75A2-652)

JOURNAL OF RESEARCH of tae National Bureau of Standards—A. Physics and Chemistry
Vol. 75A, No. 2, March–April 1971

Table of Spin-Orbit Energies for *p*-Electrons in Neutral Atomic (core)*np* Configurations

W. C. Martin

Institute for Basic Standards, National Bureau of Standards, Washington, D.C. 20234

(November 23, 1970)

Data are given in support of the recently proposed formula $\zeta_{np}n^{*3}=0.450Z^{2.33}$ cm^{-1} ($Z \geq 5$). The table includes evaluations of this formula, which are probably accurate to ~ 15 percent for all atoms $Z=10$ to 90. For many (core)*np* configurations, the accuracy of ζ_{np} from the formula is greater than that to be expected from fitting the observed levels to intermediate coupling theory.

Key words: Atomic spectra; atomic theory; spin-orbit interaction.

1. Introduction

Values of the spin-orbit coupling parameter ζ_{np} for configurations of the type (core)*np* in neutral atoms were recently shown to be fairly accurately reproduced for atomic numbers $Z \geq 5$ by the formula [1][1]

$$\zeta_{np}n^{*3}=0.450Z^{2.33}\ \text{cm}^{-1}, \qquad (1)$$

where n^* is the effective principal quantum number of the *np* electron. The relation of the Z-dependence of the spin-orbit interaction to its physical origin was discussed in [1]. This note gives in more detail some data supporting the formula, and evaluations of it for $Z \leq 90$.

2. Values of $\zeta_{np}n^{*3}$

The dependence $\zeta_{np} \propto 1/n^{*3}$ is known to be a good approximation for simple spectra [2, 3, 4]. The change in n^* corresponding to the fine structure splitting is thus approximately constant for a series with structure proportional to ζ_{np} (*np* ^2P and *snp* $^3P_{2-0}$ intervals) [2, 4]. Observations of unperturbed series of this type usually show Δn^* to be constant within ~ 2 percent, except for the lowest series member or two.

The constants in (1) were determined by graphically fitting the data from such series in ten spectra,[2] indicated by stars after the element symbols in table 1. The series members that determined the value of $\zeta_p n^{*3}$ for each of these spectra are listed under the heading "*np* Data." These ten spectra range in atomic number from 11 to 81, with an average disagreement of 6 percent between the observed value of $\zeta_p n^{*3}$ and the value from (1). The maximum disagreement is 12 percent.

The other data in the table are less reliable.[3] Most configurations of the type (core)*np* with the core including a partly filled *p* or *d* subshell appear to be distorted by perturbations that are significant compared to ζ_{np}. The data were usually taken from the lowest such configuration, to minimize the relative error in ζ_p. The $\zeta_p n^{*3}$ values for these lowest configurations are systematically larger than the limiting constant values (from eq (1)) by ~ 15 percent. At least part of this effect is understood [3, 1]. Part of the remaining scatter in these values is probably due to configuration interactions neglected in the calculations. In some spectra there may also be uncertainty in obtaining properly corresponding values of ζ_p and n^* [1].

It seems likely that the formula values of $\zeta_p n^{*3}$ (table 1) are correct to ~ 15 percent for (core)*np* configurations (*n* greater than any principal quantum number in the core) in all atoms $Z=10$ to 90. This accuracy must of course not be expected if perturbation has affected the value of n^{*3} by more than a few percent. Any other large percentage deviations from the formula are suspect and probably unphysical. In many cases rather complete and detailed calculations would be necessary to obtain values of ζ_p by the level-fitting method as accurate as the formula values. It would thus be advantageous in some instances to fix this parameter.

Some examples of these various points may be inferred from table 2, where values of ζ_p obtained by different methods for several rare-gas configurations are compared. The smaller values of ζ_p, as in Ne, are

[1] Figures in brackets indicate the literature references at the end of this paper.

[2] It is notable that the data for eight of these spectra are from accurate observations made in Lund, Sweden, during the past 15 years.

[3] Only a representative selection of the data available from complex spectra is given in the table. The $\zeta_p n^{*3}$ values listed for the first few elements following hydrogen are not accurate, since other interactions that contribute significantly to the term intervals were not allowed for. The results and discussion are not applicable for $Z \leq 5$.

TABLE 1. *Values of ζn^{*3} for* np*-electrons in configurations of the type* (*core*) np.

The data are from neutral atoms with the core-configurations shown. A core with electrons of different *nl* indicates that configuration interaction was included in the calculation. Where more than one *np* electron is shown in the fourth column, the value in the fifth column is an average. References for data or calculations are indicated by letters in parentheses in the fourth column. The other experimental values of ζn^{*3} are based on data from *Atomic Energy Levels* [C. E. Moore, Nat. Bur. Stand. (U.S.), Circ. 467, Vol. I (1949); Vol. II (1952); Vol. III (1958)].

Z	Atom	Core	*np* Data	ζn^{*3} Data	ζn^{*3} Formula
				(cm^{-1})	(cm^{-1})
1	H		*np*	1.94	0.45
2	He	$1s$	$2p$	5.16	2.26
3	Li	$1s^2$	$2p$	1.68	5.8
4	Be	$2s$	$2p$	6.00	11.4
5	B	$2s^2$	2, $3p$	19.3	19.1
6	C	$2p$			29.3
7	N	$2p^2$			41.9
8	O	$2p^3$			57
9	F	$2p^4$			75
10	Ne	$2p^5$			96
11	Na*	$2p^6$	4–8p[a]	117	120
12	Mg*	$3s$	4–6p[b]	149	147
13	Al*	$3s^2$	4–7p[c]	200	177
14	Si	$3p$			211
15	P	$3p^2$			247
16	S	$3p^3$			288
17	Cl	$3p^4$			331
18	Ar	$3p^5$			378
				(10^2 cm^{-1})	(10^2 cm^{-1})
19	K*	$3p^6$	5–10p[a]	4.39	4.29
20	Ca*	$4s$	5–8p[d]	5.1	4.84
21	Sc	$(3d+4s)^2$			5.4
22	Ti	$(3d+4s)^3$			6.0
23	V	$(3d+4s)^4$			6.7
24	Cr	$(3d+4s)^5$			7.4
25	Mn	$(3d+4s)^6$			8.1
26	Fe	$(3d+4s)^7$			8.9
27	Co	$(3d+4s)^8$			9.7
28	Ni	$(3d+4s)^9$	4p[e]	13.0	10.6
29	Cu	$(3d+4s)^{10}$	4p[f]	12.5	11.5
30	Zn*	$4s$	5–8p[g]	11.0	12.4
31	Ga*	$4s^2$	5–7p[h]	14.0	13.4
32	Ge	$4p$	5p[i]	15.9	14.5
33	As	$4p^2$			15.5
34	Se	$4p^3$			16.7
35	Br	$4p^4$			17.8
36	Kr	$4p^5$	6p[i]	21.8	19.0
				(10^3 cm^{-1})	(10^3 cm^{-1})
37	Rb*	$4p^6$	7–11p[j]	1.92	2.03
38	Sr	$5s$	5p	2.55	2.16
39	Y	$(4d+5s)^2$			2.29
40	Zr	$(4d+5s)^3$			2.43
41	Nb	$(4d+5s)^4$			2.58
42	Mo	$(4d+5s)^5$			2.73
43	Tc	$(4d+5s)^6$			2.88
44	Ru	$(4d+5s)^7$			3.04
45	Rh	$(4d+5s)^8$			3.20
46	Pd	$(4d+5s)^9$			3.37
47	Ag	$4d^{10}$	6p	3.47	3.54
48	Cd	$5s$	6p	3.58	3.72
49	In	$5s^2$	6, 7p[h]	3.99	3.90
50	Sn	$5p$			4.09
51	Sb	$5p^2$			4.28
52	Te	$5p^3$			4.48
53	I	$5p^4$			4.69
54	Xe	$5p^5$	6p[k]	4.79	4.89
55	Cs*	$5p^6$	8–13p	4.74	5.1
56	Ba	$6s$	6p	6.1	5.3
57	La	$(5d+6s)^2$			5.6
58	Ce				5.8
59	Pr				6.0
60	Nd	$4f^4 6s$			6.3
61	Pm	$4f^5 6s$			6.5
62	Sm	$4f^6 6s$			6.8
63	Eu	$4f^7 6s$	6p[l]	8.3	7.0
64	Gd	$4f^7 5d 6s$			7.3
65	Tb				7.5
66	Dy	$4f^{10} 6s$			7.8
67	Ho	$4f^{11} 6s$			8.1
68	Er	$4f^{12} 6s$			8.4
69	Tm	$4f^{13} 6s$			8.7
70	Yb	$6s$	6p	10.5	9.0
71	Lu	$(5d+6s)^2$			9.3
72	Hf	$(5d+6s)^3$			9.6
73	Ta	$(5d+6s)^4$			9.9
74	W	$(5d+6s)^5$			10.2
75	Re	$(5d+6s)^6$			10.5
76	Os	$(5d+6s)^7$			10.9
77	Tr	$(5d+6s)^8$			11.2
78	Pt	$(5d+6s)^9$			11.5
79	Au	$5d^{10}$	6p	14.4	11.9
80	Hg	$6s$	6p	17.8	12.2
81	Tl*	$6s^2$	7–11p	13.4	12.6
82	Pb	$6p$			13.0
83	Bi	$6p^2$			13.3
84	Po	$6p^3$			13.7
85	At	$6p^4$			14.1
86	Rn	$6p^5$			14.5
87	Fr	$6p^6$			14.9
88	Ra	$7s$	7, 8p	18.2	15.3
89	Ac	$(6d+7s)^2$			15.7
90	Th				16.1

[a] Risberg, P., Arkiv Fysik **10,** 583 (1956).
[b] Risberg, G., Arkiv Fysik **28,** 381 (1965).
[c] Eriksson, K. B. S., and Isberg, H. B. S., Arkiv Fysik **23,** 527 (1963).
[d] Risberg, G., Arkiv Fysik **37,** 231 (1968).
[e] Roth, C., J. Res. Nat. Bur. Stand. (U.S.), **74A** (Phys. and Chem.) 715–722 (Sept.–Oct. 1970).
[f] Landman, D. A., Levin, L. A., and Lurio, A., J. Opt. Soc. Am. **59,** 962 (1969).
[g] Johansson, I., and Contreras, R., Arkiv Fysik **37,** 513 (1968).
[h] Johansson, I., and Litzén, U., Arkiv Fysik **34,** 573 (1967).
[i] Cowan, R. D., and Andrew, K. L., J. Opt. Soc. Am. **55,** 502 (1965).
[j] Johansson, I., Arkiv Fysik **20,** 135 (1961).
[k] Liberman, S., J. phys. **30,** 53 (1969).
[l] Smith, G., and Wybourne, B. G., J. Opt. Soc. Am. **55,** 121 (1965).

TABLE 2. *Values of spin-orbit energy for* np *electrons in some rare-gas configurations.*

The "formula" values of ζ_{np} (from ζn^{*3} in table 1) are probably accurate to 15 percent.

Core		np	n^*	ζ_{np}, cm^{-1}	
				Formula	Level-fitting Calculations
Ne	$2p^5$	$3p$	2.154	9.6	[a]40.0, [b]13 ± 60
		$4p$	3.163	3.0	[b]1 ± 12
		$5p$	4.165	1.33	[a]8.1
		$6p$	5.165	0.70	[a]5.4
Ar	$3p^5$	$4p$	2.279	32	[b]28 ± 29, [c]32.6
		$5p$	3.306	10.5	[a]44.1, [b]16 ± 7, [c]13.2
		$6p$	4.310	4.7	[a]7.1
Kr	$4p^5$	$5p$	2.322	152	[a]246, [b]159 ± 25
		$6p$	3.356	50	[a]49.0, [b]58 ± 9
Xe	$5p^5$	$6p$	2.383	361	[a]374, [d]353.7

[a] Condon, E. U., and Shortley, G. H., The Theory of Atomic Spectra, pp. 306–312 (Cambridge, 1953). Some of these values were quoted from earlier calculations, with references given.

[b] Cowan, R. D., and Andrew, K. L., J. Opt. Soc. Am. **55,** 502 (1965).

[c] Garstang, R. H., and Van Blerkom, J., J. Opt. Soc. Am. **55,** 1054 (1965).

[d] Liberman, S., J. Phys. **30,** 53 (1969). Calculation includes interaction with $5p^57p$.

relatively more sensitive to distortion by perturbations in level-fitting determinations.

The core configurations listed in table 1 are the lowest for each element. (A few of the cores that have low levels of both parities are not listed.) However, the value of ζ_{np} is only weakly affected by core excitation for most configurations observed in optical spectroscopy. Values of n^* for a particular np (n greater than for any core electron) but based on different core configurations will normally differ by fairly small amounts if the configurations involved are unperturbed. The most reliable experimental values of n^* are usually obtained from terms based on the core configurations in the table.

The available data would probably yield useful relations for the Z-dependence of $\zeta_p n^{*3}$ in ionized spectra. Both this and the probably more troublesome extension to higher l [1] would merit investigation.

3. References

[1] Fano, U., and Martin, W. C., in Topics in Modern Physics, A Tribute to E. U. Condon (Brittin, W. E., and Odabasi, H., eds., Colorado Associated University Press, 1971).

[2] Landé, A., Z. Physik **25,** 46 (1924).

[3] Casimir, H. B. G., Arch. Musée Teyler, Series 3, **8,** 201 (1936).

[4] Edlén, B., "Atomic Spectra" in Encyclopedia of Physics, S. Flügge, Ed., Vol. **27,** pp. 129–130 (Springer-Verlag, Berlin, 1964).

(Paper 75A2–653)

JOURNAL OF RESEARCH of the National Bureau of Standards — A. Physics and Chemistry
Vol. 75A, No. 2, March–April 1971

Heat Capacities of *cis*-1,4-Polyisoprene from 2 to 360 K

S. S. Chang and A. B. Bestul*

Institute for Materials Research, National Bureau of Standards, Washington, D.C. 20234

(November 24, 1970)

Heat capacities of amorphous synthetic *cis*-1,4-polyisoprene have been determined for the quenched and annealed glasses from 2 to T_g (around 200 K) and for the liquid from T_g to 360 K, with a precision of better than 0.05 percent above 15 K. T_g, as determined from H versus T plots, is 203 K for the quenched glass and 198 K for the annealed glass. For the glasses the heat capacity values from this research are about 1 percent higher than that reported in 1935 for natural rubber hydrocarbon. For the liquid the result from this research agrees better (within 1 percent) with recently (1967) proposed values than those from the earlier experiment cited. Effects of crystallization and melting, stark rubber crystals, and additives (antioxidants and stabilizers) were also studied.

Key words: Annealed and quenched glass; calorimetry; glass transformation; heat capacity; natural rubber; normal and supercooled liquid; *cis*-1,4-polyisoprene; rubber, natural; thermal diffusivity; thermodynamic properties.

1. Introduction

Heat capacities of natural rubber hydrocarbon from 14 to 320 K were reported by Bekkedahl and Matheson in 1935 [1].[1] After several decades, a review by Gehman [2] on the thermal diffusivity of natural rubber showed discrepancies which Wood and Bekkedahl [3] explained by the suggestion that Bekkedahl and Matheson's values for the temperature dependence of the heat capacity were too high around room temperature, and too low at lower temperatures. They proposed that the 1935 heat capacity results had been affected by undetected crystallization effects, which were little understood at the time of those measurements. On the basis of more recent knowledge of crystallization in natural rubber, they proposed adjustments to the 1935 data to bring it into greater consistency with current thermal diffusivity values.

To provide a new experimental basis for these heat capacities, the present paper reports new determinations for *cis*-1,4-polyisoprene from 2 to 360 K with a precision of about 0.05 percent of the values over most of that range. The effects of quenching and annealing on the heat capacity of the glass and on the glass transformation temperature were also studied.

The *cis*-1,4-polyisoprene sample investigated was the synthetic product rather than the natural product. Although the synthetic polymer contains about 3 percent of the 3,4-adduct as compared with a typical value of 2 percent for the natural polymer, the synthetic sample was chosen for the two following reasons. The natural product requires a much more complicated and uncertain purification process. Also the synthetic polymer crystallized much more slowly than the natural polymer [4], thus making it much easier to avoid the crystallization effects which are thought to have affected the 1935 measurements [1].

2. Experimental Detail

2.1. Apparatus

The heat capacity measurements reported here were performed in the vacuum adiabatic calorimeter described previously [5]. The measuring procedures and methods of data treatment, especially for the glass transformation region, were discussed in more detail in a previous paper [6], where several modifications on the instruments were also described.

The following additional modifications have now been made in the apparatus:

By pumping on the liquid helium reservoir, the calorimeter can now be cooled to 1.8 K and maintained there for 5 to 6 hours. The mechanical choppers of the adiabatic shield control system are replaced by photochoppers, and the outputs from the power amplifiers are rectified and filtered before being fed to the shield heater.

Constant current supplies, capable of supplying 1 to 10 mA with stabilities in the order of 1 ppm, are used instead of batteries to energize the platinum resistance thermometer and its measuring potentiometer. This eliminates the necessity of readjusting the potentiometer and the thermometer currents during a day of measurements. The drift in the thermometer

*Present address: Office of Special Studies, National Oceanographic and Atmospheric Administration, 6010 Executive Blvd., Rockville, Md. 20852.

[1] Figures in brackets indicate the literature references at the end of this paper.

413-992 O - 71 - 2

potential now reflects only the change in the temperature of the thermometer element, without any additional change in the thermometer current. A nanovolt null detector is used instead of the photoelectric galvanometer. This detector recovers from a large overvoltage at its input in a few seconds, whereas a galvanometer coil sticks off scale. Connections between circuit modules are made with barrier-type terminal strips. In critical circuits, gold-plated copper shorting links and washers are used on the terminal strips to avoid the generation of thermal emf's. Multiple-gang low thermal emf silver-alloy wafer switches are used as the master selector switch, the range switch, and the reversing switch. The master selector switch controls the application of electrical energy to the calorimeter heater, turns the heater timer on and off synchronously with the energy, and selects either the heater or the thermometer for the potentiometer input. The range switch adjusts the heater circuit voltage divider network, composed of calibrated standard resistors, to maintain the signal near the 0.1-V full-scale reading of the potentiometer. The reversing switch is used to reverse the polarities of all power supplies at their terminals. Thus the residual emf in a circuit can be checked without disturbing the connections for emf input to, and for detector output from, the potentiometer. With room temperature maintained within 1 °C and potentiometer corrections applied from inter-dial comparisons, the accuracy for the entire potentiometric system is better than 2 ppm for the ratio of potentials involved in the resistance ratio measurement, and better than 10 ppm for an individual potential measurement. As the thermometric potentiometer system measures liquid helium temperatures, the null detector can resolve 5 nV, and around room temperature the resolution is about 10 nV. The resistance of the platinum resistance thermometer, including that of the leads, varies from 3 to 50 Ω over the temperature range of the measurements. Thus the 25-Ω (at 0 °C) platinum resistance thermometer, excited by a 2 mA current above 40 K, and below this by higher currents up to 10 mA at 2 K, yields a resolution in temperature better than 5×10^{-3} K at 2 K, 5×10^{-4} K, at 10 K, and 5×10^{-5} K above 40 K. The output of the nanovoltmeter is recorded on a strip chart. A full scale of $\pm1\mu$V is normally used, which is equivalent to a 0.01 K span above 40 K.

A constant current supply, with high power rating and 10 ppm stability, was used as the energy source for the calorimeter heater.

The platinum resistance thermometer was originally calibrated in accordance with the International Practical Temperature Scale (IPTS) of 1948 and the NBS–1955 provisional scale. This calibration has been adjusted so it conforms with the IPTS–1968 [7, 8] above 13.81 K. Between 2 to 20 K, this platinum thermometer was compared against germanium thermometer S/N 1466 which has been calibrated through the same range by the Temperature Section of NBS in accordance with the NBS–1965 (2 to 20 K) provisional scale [9]. The result of the comparison was fitted to a fifth-degree polynomial [10] which was then used to calculate temperatures of the platinum thermometer between 2 to 14 K. The use of the new temperature scale eliminates the mini-maximum in the heat capacities around 70 and 90 K which was caused by the old temperature scales in some previous data [6, 11, 12].

The heat capacities used for the empty calorimeter have been redetermined experimentally based on the new temperature scale.

2.2. Sample

The sample of synthetic *cis*-1,4-polyisoprene was supplied by the Goodyear Tire and Rubber Co. through the courtesy of S. D. Gehman and E. Schoenberg. The sample was in the form of a rough sheet about ½ in thick. It was translucent, having pale yellow color. The ash content of the sample was determined from spectroscopic analysis of the ashes by the Analytical Chemistry Division of NBS as 0.11 percent, with titanium and aluminum as the major components. The following information about the sample was given by the supplier: The dilute solution viscosity was 6.4 dl/g in toluene at 30 °C. The polymer was composed of 97.0 percent *cis*-1,4 adducts and 3.0 percent 3,4 adducts. To 100 parts of polymer, 0.93 parts of antioxidant and 0.20 parts of stabilizer were added. These additives were of cresol and amine types with overall weight ratio C:N:H:O = 77:7:10:6.

The calorimetric sample consisted of four annuli, weighing 68.608 g in vacuo. The weighings were carried out on a single-pan balance, designated NBS 166591, with a capacity of 1 kg and a sensitivity of 0.1 mg. The annuli, 2 in in o.d. and ½ in i.d., were punched from the sheet. The sample container was surrounded by a water-cooled jacket while the cover was soldered to the container with low melting In-Sn solder, so the sample would not heat up and would remain as closely as possible to "as received" condition. Helium gas at 10 cm Hg pressure at room temperature was sealed into the container to increase thermal conduction within it.

The heat capacity of the sample was first determined in the as received condition. When the sample was subjected to a temperature above room temperature for the first time, the heat capacities showed a broad peak, about 1.5 percent higher than the base observed later, centering around 315 K. The height of the peak diminished as the sample was recycled to successively higher temperatures up to 330 K. After the sample had been heated above 330 K, the heat capacity in the region between 290 and 330 K remained constant within 0.05 percent upon further thermal treatment. X-ray powder patterns indicated the existence of small amounts of stark rubber [13] at a barely detectable level in the original sample. Thus this initial peak was probably due to the melting of these stark rubber crystals [14]. The amount of heat represented by the peak is about 60 J/mol. This amount of heat corresponds to an estimated content of stark rubber around 1.5 percent if the heat of fusion for stark rubber is as-

sumed to be equal to that for ordinary rubber crystal [15].

After the heat capacity had been measured for the sample in the as received condition, most of the additives were removed by vacuum distillation. The calorimetric sample, while still in the sample container, was maintained at 80 °C in high vacuum for 24 days. The collected distillate was a mixture composed mainly of transparent crystals and of some yellow liquid. The total weight loss was 0.726 g or 1.06 percent. The weight of the additives in the sample, calculated from the information given by the supplier, was 0.77 g or 1.12 percent of the sample. Hence the weight loss on pumping the sample amounted to 95 percent of the weight of the additives. 1,2-dichloroethane solutions containing from 0.1 to 1 percent of the sample, before and after the pumping process, were centrifuged, filtered, and analyzed by UV spectrometry. The spectra indicated approximately a ten-fold diminishing in the absorption at 270 to 280 nm, probably due to alkylated phenols. Naphthyl group absorption in the region of 309 nm was not observed either before or after pumping on the sample. Helium gas at 10 cm Hg pressure at room temperature was again sealed in with the sample to provide good thermal contact.

Heat capacity measurements reported here in detail were made on this purified sample. These results differed very slightly from the values obtained from the sample in as received condition. The difference in heat capacity per unit weight was less than 0.1 percent over most of the temperature range investigated, except below 10 K. No shift in glass transformation temperature was detected. Hence the effective heat capacity of the additives was within 10 percent of the heat capacity of the samples, and apparently the additives did not act as plasticizers.

The quenched glass was produced by cooling at a rate of about 5 K/min through the glass transformation range. The annealed glass was produced by first cooling at a rate of about 1 K/hr (rate annealing) through the glass transformation range, and then holding at 195 K (soak annealing) for two days, when thermal drift became negligible.

3. Results

Heat capacity data for *cis*-1,4-polyisoprene are listed in table 1 and shown graphically in figure 1. The table is divided into sections for annealed glass, quenched glass, and liquid. Each section is composed of several series of continuous determinations, and is arranged in the order of increasing initial temperature of each series. These series are numbered chronologically so that the thermal history of the sample may be followed. More than one physical state may be involved in a series. The approximate temperature increment for each determination may be inferred from the temperature differences between the adjacent determinations. The temperature rise for each determination is generally 1 degree below 10 K, 10 percent of the temperature up to 100 K, and 10 degrees above 100 K. Deviations of individual values from the smoothed curves for the respective physical forms are shown in figure 2. The precision of measurement is better than 0.05 percent above 15 K and gradually changes to 1 to 2 percent at 2 K. Although the accuracy of the measurement was shown to be comparable with the precision [5], estimated error for this sample is probably greater than the precision because of the remaining additives and the content of 3,4-adducts.

TABLE 1. *Heat capacity data for* cis-*1,4-polyisoprene*

(base mole $[-C_5H_8-] = 68.119$)

ANNEALED GLASS

T	C_p	T	C_p	T	C_p
SERIES X		SERIES IX		SERIES XII	
K	*J/K/mol*	*K*	*J/K/mol*	*K*	*J/K/mol*
2.50	.046	30.81	14.67	157.09	63.53
2.99	.086	34.01	16.88	167.15	66.70
3.61	.161	37.55	18.29	177.33	69.92
4.32	.281	41.50	20.30	187.42	73.16
5.05	.444	45.84	22.34	194.81	76.41
5.79	.644	50.42	24.53	199.60	78.62
6.53	.887	55.41	26.81	203.44	133.50
7.27	1.156	60.95	29.23		
8.01	1.456	67.11	31.82		
8.79	1.807	73.94	34.62		
9.64	2.207	SERIES XI			
10.56	2.672				
11.65	3.257	79.40	36.78		
12.91	3.975	87.64	39.98		
14.13	4.618	98.47	43.98		
		107.77	47.28		
15.37	5.429	117.36	50.59		
16.89	6.355				
18.58	7.409	127.04	53.83		
20.33	8.491	136.99	57.07		
22.27	9.688	147.10	60.33		
24.46	11.02				
26.85	12.43				
29.52	13.94				
32.64	15.67				
35.98	17.47				

QUENCHED GLASS

SERIES V		SERIES VI		SERIES VIII	
2.22	.032	27.72	12.95	153.81	62.72
2.63	.057	30.72	14.63	163.51	65.83
3.21	.112	33.65	16.25	173.46	69.02
3.91	.210			183.58	72.16
4.65	.355	SERIES III		193.47	76.65
5.39	.540	68.01	32.24	200.68	85.68
6.13	.762	73.46	34.46	204.84	109.05
6.89	1.026	79.28	36.77		
7.67	1.332	85.48	39.19		
8.47	1.674	92.06	41.68		
9.26	2.045	100.00	44.58		
10.06	2.438	109.31	47.89		

TABLE 1. *Heat capacity data for* cis-*1,4-polyisoprene*—Continued

(base mole $[-C_5H_8-] = 68.119$)

QUENCHED GLASS—Continued

T	C_p	T	C_p	T	C_p
SERIES VII		SERIES IV			
4.64	.354	119.83	51.54		
5.40	.545	129.27	54.69		
6.17	.775	138.76	57.80		
6.96	1.057	148.44	60.94		
7.79	1.381				
8.66	1.766				
9.63	2.226				
10.67	2.755				
11.78	3.356				
12.97	4.040				
14.24	4.766				
15.62	5.618				
17.18	6.570				
18.89	7.632				
20.69	8.741				
22.71	9.977				
25.02	11.38				
27.78	13.02				
30.79	14.67				
34.07	16.48				
37.77	18.41				
41.69	20.38				
45.83	22.38				
50.32	24.50				
55.49	26.86				
61.20	29.36				
67.16	31.87				
73.31	34.40				

LIQUID

SERIES XII		SERIES II	
209.03	110.85	276.18	124.50
214.82	111.85	286.07	126.82
		295.82	129.17
SERIES VIII		305.44	131.46
		314.92	133.87
210.53	111.05		
		SERIES XIV	
SERIES XIII			
		317.22	134.32
221.18	112.99	326.56	136.63
230.50	114.77	335.78	138.91
240.08	116.65	345.48	141.32
249.90	118.87[a]	355.24	143.73
259.78	121.10[a]		
		SERIES I	
269.70	123.73[b]		
279.65	125.43	344.83	141.03
289.47	127.69	354.17	143.36
299.17	130.00		
308.73	132.32		

[a] less accurate assignment of quasi-adiabatic drift due to crystallization.

[b] fusion included.

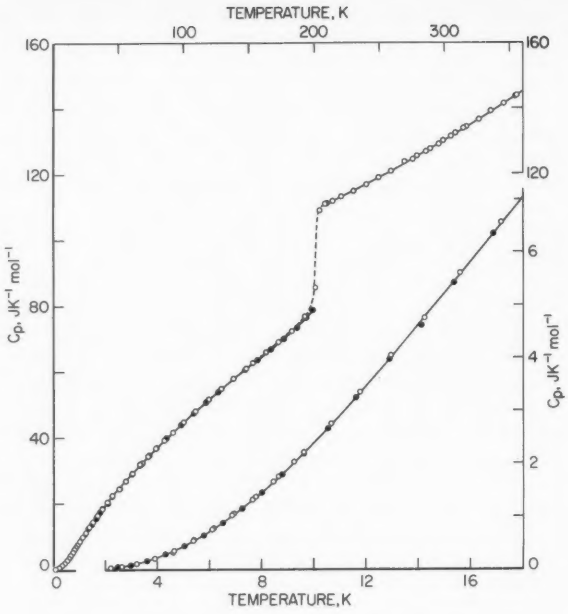

FIGURE 1. *Heat capacities of* cis-*1,4-polyisoprene.*

• annealed glass, ◦ quenched glass and liquid.

Smoothed heat capacity values at rounded temperatures are listed in table 2, along with enthalpy and entropy integrals referenced to the annealed glass at 0 K. The values for the quenched glass are placed on this reference by first integrating and summing the data for the annealed glass from 0 K up to 210 K, where the sample is in the equilibrium liquid state and has thermodynamic properties independent of thermal history. From this point, the data for the quenched glass are then summed and integrated back down to the temperatures listed in table 2. The glasses are expected to have undetermined residual entropies at 0 K; hence the entropy and enthalpy increments listed in table 2 cannot be combined to give a Gibbs free energy.

Plots of C_p/T^3 versus T^2 for both glasses below 15 K are shown in figure 3. They show pronounced peaks between 4 and 5 K for both glasses. Clearly the glasses have not yet reached the Debye T^3 region even at 2 K. Entropy and enthalpy increments between 0 and 2 K are however estimated by means of a T^3 dependence of the heat capacity. These estimates, which amount to 0.011 J/mol for the enthalpy and 0.008 J/K/mol for the entropy, should not introduce any significant error in the respective integrals.

The heat capacity of the quenched glass is higher than that of the annealed glass throughout the entire temperature range of measurement. The difference is about 1 to 2 percent below 15 K; it decreases to 0.1 percent between 35 to 100 K and then increases to 1 percent at 190 K. The heat capacities of the glasses from this research are about 1 percent higher than those from reference [1] between 70 and 200 K and increase to 4 percent higher at 15 K.

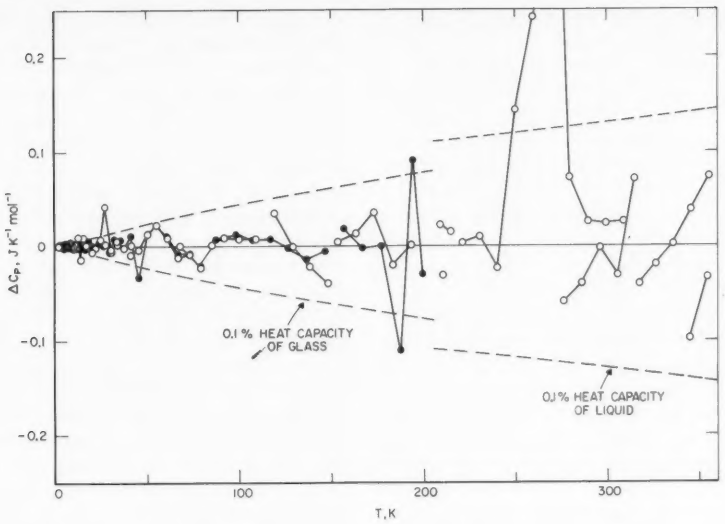

FIGURE 2. *Deviations of individual heat capacity determinations for* cis-*1,4-polyisoprene from smoothed curves.*

• annealed glass, ◦ quenched glass and liquid.

TABLE 2. *Thermodynamic functions of* cis-*1,4-polyisoprene*

(Units in K, J and mol; $[-C_5H_8-] = 68.119$)

ANNEALED GLASS			
T	C_p	$H-H_0^{AG}$	$S-S_0^{AG}$
0		[0]	[0]
2	0.023	0.011	0.008
5	0.43	0.53	0.14
10	2.39	7.03	0.96
15	5.21	25.82	2.45
20	8.29	59.52	4.37
25	11.34	108.65	6.55
30	14.22	172.62	8.87
35	16.94	250.6	11.27
40	19.56	341.9	13.70
45	21.98	445.8	16.15
50	24.33	561.6	18.59
60	28.81	827.5	23.42
70	33.03	1136.8	28.18
80	37.03	1487.3	32.86
90	40.86	1876.9	37.44
100	44.52	2304.	41.94
110	48.05	2767.	46.35
120	51.48	3265.	50.67
130	54.81	3796.	54.93
140	58.06	4361.	59.11
150	61.27	4957.	63.22
160	64.44	5586.	67.28
170	67.60	6246.	71.28
180	70.68	6937.	75.23
190	74.27	7661.	79.14
200	78.85	8426.	83.07
210 (liq.)		[9595.]	[88.77]

TABLE 2. *Thermodynamic functions of* cis-*1,4-polyisoprene*—Continued

(Units in K, J and mol; $[-C_5H_8-] = 68.119$)

QUENCHED GLASS			
T	C_p	$H-H_0^{AG}$	$S-S_0^{AG}$
0		[171.7]	[0.77]
2	0.023	171.7	0.78
5	0.44	172.2	0.92
10	2.41	178.8	1.75
15	5.23	197.7	3.25
20	8.32	231.6	5.17
25	11.36	280.8	7.36
30	14.24	344.9	9.69
35	16.97	423.0	12.09
40	19.54	514.3	14.52
45	21.99	618.2	16.97
50	24.34	734.1	19.41
60	28.83	1000.	24.25
70	33.06	1310.	29.01
80	37.07	1660.	33.69
90	40.90	2050.	38.28
100	44.58	2478.	42.78
110	48.12	2941.	47.19
120	51.57	3440.	51.53
130	54.93	3973.	55.79
140	58.23	4538.	59.98
150	61.48	5137.	64.11
160	64.70	5768.	68.18
170	67.89	6431.	72.20
180	71.06	7126.	76.17
190	74.85	7855.	80.11
210 (liq.)		[9595.]	[88.77]
LIQUID			
210	110.99	9595.	88.77
220	112.77	10715.	93.97

TABLE 2. *Thermodynamic functions of* cis-*1,4-polyisoprene*—Continued

(Units in K, J and mol; $[-C_5H_8-]=68.119$)

LIQUID—Continued			
T	C_p	$H-H_0^{AG}$	$S-S_0^{AG}$
230	114.67	11851.	99.03
240	116.66	13008.	103.95
250	118.74	14184.	108.76
260	120.91	15383.	113.45
270	123.15	16603.	118.06
280	125.44	17846.	122.58
290	127.79	19112.	127.02
300	130.18	20402.	131.39
310	132.60	21716.	135.70
320	135.04	23054.	139.87
330	137.49	24416.	144.14
340	139.94	25803.	148.28
350	142.38	27215.	152.38
360	144.81	28651.	156.42
273.15	123.86	16992.	119.49
298.15	129.74	20161.	130.59

3.1. Glass Transformation

Enthalpy changes as functions of temperature through the glass transformation range are shown in figure 4. The enthalpy of the quenched glass is about 195 J/mol higher than that of the annealed glass at 200 K and about 172 J/mol at 0 K. The corresponding entropy differences are 1.04 and 0.77 J/K/mol, respectively.

The glass transformation temperature T_g, defined as the temperature of intersection of the extrapolated enthalpy versus temperature curves from the equilibrium supercooled liquid and the configurationally fixed glasses, is 203 K for the quenched glass and 198 K for the annealed glass. The extrapolation of the well-behaved liquid curve should not introduce appreciable error. During the normal measuring process a well-annealed glass tends to maintain fixed configurations up through its T_g. Hence the T_g of annealed glass can easily be so determined. For the quenched glass, energy releases due to configurational change can be detected as far as 40 deg below the T_g. Hence in constructing the enthalpy curve for the quenched glass at such temperatures for a configurationally fixed state, preference is given to the initial enthalpy-temperature relation of the sample immediately after an energy input. Also the slope of the enthalpy curve for the annealed glass is taken as a lower limit for that of the quenched. The elongated data points in figure 4 indicate the extent of temperature change occurring during a typical drift period of about 1 hr. The combined enthalpy of the sample and of the sample container remains fixed during the drift period. However, the enthalpy of the sample shows either a loss or gain due to the corresponding gain or loss in the enthalpy of the sample container with changing temperature for quenched or annealed glasses, respectively. Although T_g so defined is dependent on the thermal history by which the particular glass was produced, it is independent of the rate of observation. This method corresponds to the dilatometric method in which T_g is taken as the intercept in the volume-temperature diagram. If the inflection points or the onset of the rise in the Cp versus T curves were used as T_g, the hysteresis effect could cause an apparently higher T_g for the annealed glass than for the quenched glass.

Spontaneous adiabatic temperature drifts in the glass transformation range are shown in figure 5. Drift observations for the sample in the as received condition are also included. Positive drift, or energy release, for the quenched glass may be detected from

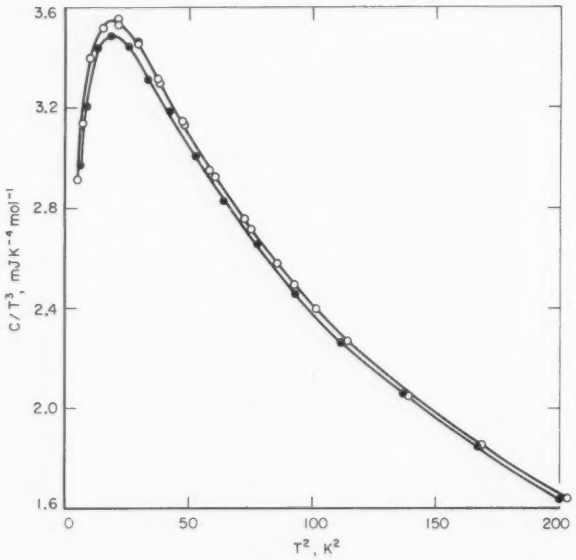

FIGURE 3. C_p/T^3 *versus* T^2 *plot for* cis-*1,4-polyisoprene below 15 K.*

• annealed glass, ◦ quenched glass.

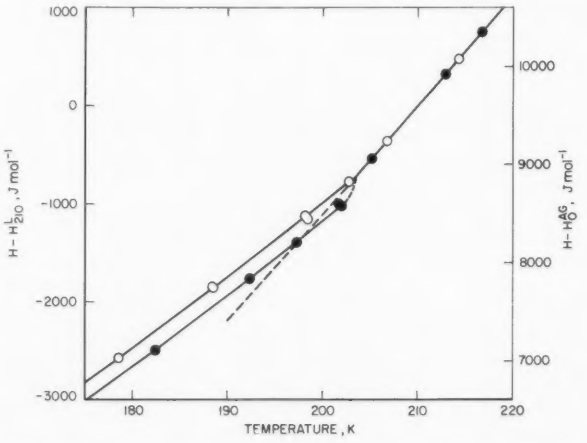

FIGURE 4. *Enthalpy changes of amorphous* cis-*1,4-polyisoprene near glass transformation region.*

• annealed glass and liquid, ◦ quenched glass and liquid.

temperatures 40 deg below T_g. Negative drift, or energy absorption, for the annealed glass started to show up just about at its T_g. These drifts indicate the directions in which the glasses tend to move themselves toward the equilibrium configurations of the supercooled liquid. The minimum in the drift at temperatures above the T_g of a annealed glass shows that the heat capacity measurement was carried out at a faster rate than the relaxation rates governing configurational changes below and at T_g. At higher temperatures the relaxation time decreases to the order of the experimental time scale. The maximum in the drift at temperatures below the T_g of a quenched glass is produced because the experimental time is long in comparison to the relaxation time for many of the configurational changes in the quenched glass. The minimum and the maximum in the drift plot correspond roughly to the inflection points in the heat capacity curves. Above 205 K an equilibrium liquid is produced within the normal experimental time irrespective of the previous history.

The difference in the heat capacities between the liquid and the glass at 200 K is 30.5 ± 0.5 J/K/mol.

3.2. Crystallization

Crystallization of the sample may be detected by warming drifts in the temperature range from 235 to 270 K. If the sample has been cooled to temperatures below T_g since its last melting, the maximum rate of energy release from the sample is about 1 mW/mol at 250 K. If the sample has not been cooled below 240 K since its last melting, the rate of energy release is much smaller, presumably due to fewer nuclei being formed. It takes about 4 hr to measure heat capacities through the crystallization region. The total energy released by the sample in this time is in the order of 10 J/mol. This energy corresponds to a degree of crystallinity of about 0.25 percent, based on a heat of fusion of 4360 J/mol obtained from the melting points of a polymer-diluent system [15].

3.3. Liquid

Except for the results of a few determinations where crystallization and fusion occurred, the heat capacity of the liquid above 205 K can be fitted by least squares to a cubic expression in T with a standard deviation of 0.035 percent. In the crystallization range of 235 to 270 K, the rate of spontaneous energy release passes through a maximum as a function of temperature. At the maximum the half-time for the crystallization is in excess of 25 hr [4]. The rate of crystallization appears to be constant at fixed temperature. The observed calorimetric drift includes both the heat release from crystallization as well as the heat leak in the calorimetric system. By extrapolating the combined drifts to the midpoint of a heating period, the heat capacity of the sample is determined with minimal effect from the crystallization process. The heat capacity so determined in the crystallization range shows a deviation on the order of 0.1 to 0.2 percent, from values interpolated from higher and lower temperatures. This is probably due to the nonlinear change in the combined drift during the heating period and to the uncertainties in determining the linear region for relatively large drifts. The small amount of crystals, produced during the heat capacity measurements in the crystallization range, can be observed to melt around 270 K. The melting process sometimes introduces a somewhat longer time constant than normal for the system to reach a steady state. However, it does not introduce an additional contribution to the quasi-adiabatic temperature drift beyond that due to the heat leak of the calorimetric system. Hence the energy required to melt the crystal cannot be eliminated from the determination of the apparent heat capacity by extrapolation of drifts. The deviation at 270 K, about 0.5 percent higher than the base, is probably due to the inclusion of the heat for melting.

A comparison of literature values [1, 3] with the result from this research as the base line is shown in

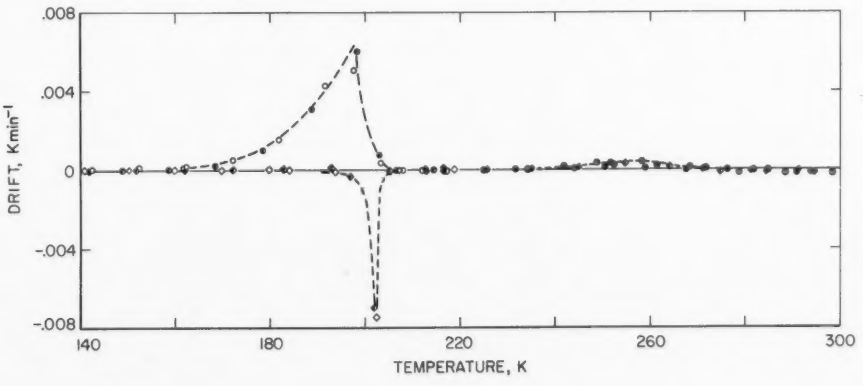

FIGURE 5. *Calorimetric temperature drifts for cis-1,4-polyisoprene near the glass transformation and the crystallization regions.*

◖ annealed glass and liquid. ◐ quenched glass. All other unfilled circles and diamonds, observations from sample before purification.

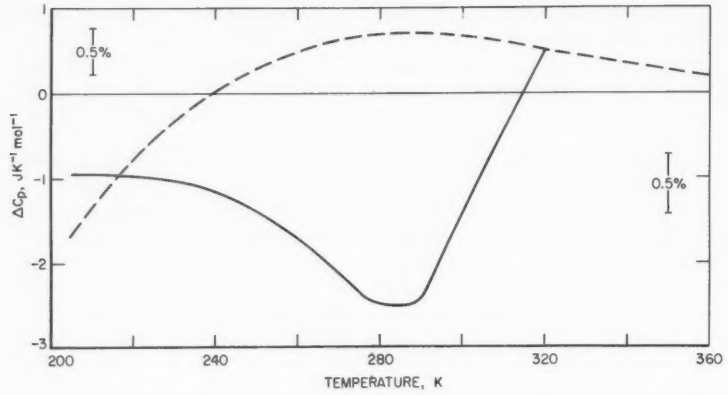

FIGURE 6. *Differences between literature values for heat capacities of* cis-*1,4-polyisoprene from smoothed values reported in this research.*

——— Bekkedahl and Matheson (1935);
- - - - - - Wood and Bekkedahl (1967).

figure 6. The solid line represents the deviation of the earlier work on natural rubber hydrocarbon [1] from ours. The deviation ranges from 1 to 2.5 percent. The dashed line represents the deviation of Wood and Bekkedahl's [3] proposed behavior for liquid natural rubber from ours. This behavior was proposed after examining heat capacities of many other liquid elastomers. It is represented by a straight line linking two points—the heat capacity at the highest temperature, 320 K, of Bekkedahl and Matheson's measurement [1], and a mean value at 100 °C over a 150-deg interval reported by McPherson and Bekkedahl [16]. Except at temperatures below 220 K, the proposed behavior is within 1 percent of the experimental values from this research.

Gehman [2] calculated the temperature coefficient of thermal diffusivity $d\alpha/dt$ of rubber at 25 °C, in 10^{-6} $cm^2/s/K$, as -1.9 using data from reference [1] and -1.15 using the proposed value from reference [3]. If the result of this research is used to estimate $d\alpha/dt$, a value of -1.18 is obtained. Results obtained both from this research and from the proposed value give closer agreement with the experimental value of -0.9 [17].

4. References

[1] Bekkedahl, N., and Matheson, H., J. Res. Nat. Bur. Stand. (U.S.), **15,** 503 (1935).

[2] Gehman, S. D., Rubber Chem. Tech. **40,** 36 (1967).

[3] Wood, L. A., and Bekkedahl, N., J. Polymer Sci. **B5,** 169 (1967).

[4] Scott, K. W., Trick, G. S., Mavor, R. H., Saltman, W. M., and Pierson, R. M., Rubber and Plastic Age **42,** 175 (1961).

[5] Sterrett, K. F., Blackburn, D. H., Bestul, A. B., Chang, S. S., and Horman, J., J. Res. Nat. Bur. Stand. (U.S.), **69C** (Eng. and Instr.), 19 (1965).

[6] Chang, S. S., Horman, J. A., and Bestul, A. B., J. Res. Nat. Bur. Stand. (U.S.), **71A** (Phys. and Chem.), 293 (1967).

[7] Comité International des Poids et Mesures, Metrologia **5,** 35 (1969).

[8] Bedford, R. E., Durieux, M., Muijlwijk, R., and Barber, C. R., Metrologia **5,** 47 (1969).

[9] Cataland, G., and Plumb, H. H., J. Res. Nat. Bur. Stand. (U.S.), **70A** (Phys. and Chem.), 243 (1966).

[10] Berry, R. J., Can. J. Phys. **45,** 1963 (1967).

[11] Furukawa, G. T., and Reilly, M., J. Res. Nat. Bur. Stand. (U.S.), **69A** (Phys. and Chem.), 5 (1965).

[12] Roder, H. M., J. Res. Nat. Bur. Stand. (U.S.), **69A** (Phys. and Chem.) 527 (1965).

[13] Roberts, D. E., and Mandelkern, L., J. Res. Nat. Bur. Stand. (U.S.), **54,** 167 (1955).

[14] Roberts, D. E., J. Res. Nat. Bur. Stand. (U.S.), **71A** (Phys. and Chem.), 225 (1967).

[15] Roberts, D. E., and Mandelkern, L., J. Am. Chem. Soc. **77,** 781 (1955).

[16] McPherson, A. T., and Bekkedahl, N., J. Res. Nat. Bur. Stand. (U.S.), **14,** 601 (1935).

[17] Frensdorff, H. H., J. Appl. Polymer Sci. **6,** 828 (1962).

(Paper No. 75A2-654)

JOURNAL OF RESEARCH of the National Bureau of Standards – A. Physics and Chemistry
Vol. 75A, No. 2, March–April 1971

Combined Low-Pressure and High-Pressure Measurements of Density and Bulk Modulus of Aviation Instrument Oil and 2-Methylbutane and Their Mixtures

James C. Houck and Peter L. M. Heydemann

Institute for Basic Standards, National Bureau of Standards, Washington, D.C. 20234

(November 24, 1970)

Dilatometric measurements were made on mixtures of aviation instrument oil and 2-methylbutane at low pressures. These results are combined with previous dilatometric and ultrasonic measurements at high pressures to give density, relative volume, and isothermal bulk modulus of the mixtures to pressures of 20 kilobars. The ratio of the adiabatic bulk modulus to isothermal bulk modulus for 2-methylbutane is also given.

Key words: Bulk modulus; compressibility; density; dilatometric measurements; high pressure; liquids; 2-methylbutane; ultrasonics.

1. Introduction

Pentane and 2-methylbutane (*i*-pentane), as well as their mixtures, are widely used as pressure-transmitting fluids [1][1] at very high pressures. Mixtures of pentane or 2-methylbutane with other fluids have been used to expand the range of hydrostatic pressure to beyond 50 kbar* [2]. Mixtures of 2-methylbutane with aviation instrument oil are used as pressure-transmitting fluids with good lubricity in the National Bureau of Standards 26 kbar piston gage.

Very little is known about the properties of these liquids and in particular their mixtures at high pressures. The density of pentane and 2-methylbutane was determined by Bridgman [3] to 9.8 kbar. In the present paper we will report on measurements of the density of mixtures of 2-methylbutane and aviation instrument oil (AIO) as a function of pressure up to their solidification region.

2. High-Pressure Ultrasonic and Dilatometric Measurements

The ultrasonic and dilatometric methods used in this laboratory for fluids at very high pressures have been described in a previous report [4] and again more extensively in reference [5]. We assume that the reader is familiar with these papers and will give only a very summary description here.

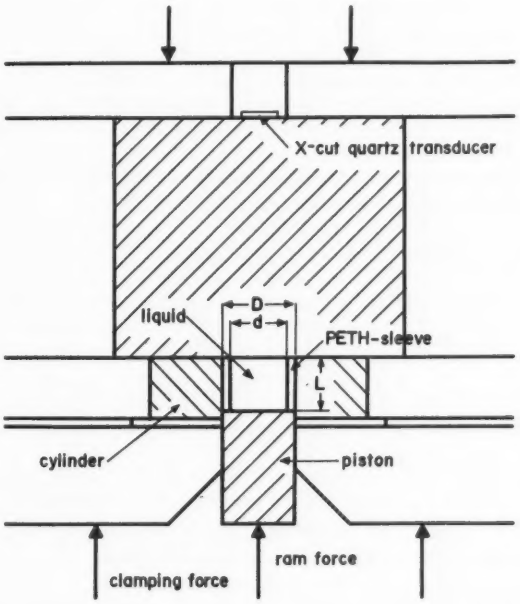

FIGURE 1. *High-pressure piston and cylinder system with fluid container.*

The high-pressure piston and die system with the polyethylene sleeve used as fluid container are shown in figure 1. Ultrasonic transit time measurements are made with the transducer cemented to the rear of the back plate. The advance of the piston into the cylinder is monitored with two dial indicators.

[1] Figures in brackets indicate the literature references at the end of this paper.
*1 kbar = 10^8 N/m^2.

The volume of the fluid at pressure p can be obtained from ultrasonic measurements carried out as a function of pressure

$$V_f(p) = V_{f0} \exp\left[-(1+\alpha_p\gamma_G T)\int_0^p \frac{dp}{B_S(p)}\right] \quad (1)$$

where $V_f(p)$, V_{f0} are the volume of the fluid at pressure p and zero;

α_p is the volume expansivity at pressure p;

γ_G is the pressure-dependent Grüneisen parameter;

T is the absolute temperature; and

$B_S(p) = \dfrac{\rho(p)L^2(p)}{\tau^2(p)}$ is the adiabatic bulk modulus with $\rho(p)$ density, $L(p)$ sample length, and $\tau(p)$ ultrasonic transit time.

An iterative procedure is used to compute increasingly better approximations of $V_f(p)$ and the length $L(p)$ of the sample. The successful solution of this problem requires knowledge of $\alpha_p\gamma_G$ as a function of pressure. It also requires knowledge of the initial dimensions of the fluid container, the amount of fluid contained, and its density and speed of sound at atmospheric pressure. If $\alpha_p\gamma_G T$ is small we may choose to neglect it. For the fluids investigated here $\alpha_p\gamma_G T$ is large at atmospheric pressure and is estimated to change rapidly with pressure. Its value as a function of pressure and temperature is not sufficiently well known to be used in the present investigation. Therefore it seems more appropriate to determine the density as a function of pressure from dilatometric measurements.

Dilatometric measurements are evaluated with the following two equations:

$$V_f(p) = \frac{D^2\pi}{4} L(p)$$

$$-\frac{D^2-d^2}{4}\pi L_0\left[1-\frac{1}{B_{1,\mathrm{PE}}}\ln\frac{B_{0,\mathrm{PE}}+B_{1,\mathrm{PE}}p}{B_{0,\mathrm{PE}}}\right] \quad (2)$$

where D, d are the outer and inner diameters of the polyethylene sleeve,

L_0, $L(p)$ are the adjusted lengths of the sleeve at ambient pressure and at pressure p, respectively,

$B_{0,\mathrm{PE}}$ is the bulk modulus of polyethylene at ambient pressure, and

$B_{1,\mathrm{PE}} = \dfrac{\partial B_{\mathrm{PE}}}{\partial p}$;

furthermore,

$$L(p) = L_0 + h_0 - h(p) + \phi\bar{p}_r + \eta\bar{p}_r^2 + \gamma[1-e^{-\epsilon\bar{p}_r}] + \beta_{\mathrm{cyl}}L_0 p \quad (3)$$

where h_0, $h(p)$ are the dial indicator readings at zero ram pressure and at pressure p;

$\phi\bar{p}_r$, $\eta\bar{p}_r^2$ are corrections for compression of the piston stack and distortion of other parts;

$\gamma[1-e^{-\epsilon\bar{p}_r}]$ is a correction for initial slack in the setup at low pressures; and

$\beta_{\mathrm{cyl}}L_0 p$ is a correction for the effect of cylinder expansion which adjusts the actual length to the length which the sample would have in a rigid cylinder, permitting the use of $L(p)/L_0$ for V/V_0.

The coefficients ϕ, η, γ, ϵ, and β_{cyl} are determined in separate experiments described in reference [5]. The zero pressure dial indicator reading, h_0, is not known since a small unknown pressure is always generated when the press is closed up. The following procedure is used to determine h_0. A value is assumed for h_0 and the bulk modulus of the sample fluid is computed from the pressure derivative of eq (2) using $L(p)$ from eq (3). We further assume that as a first approximation the bulk modulus of a sample is a linear function of pressure, at least at low pressures. We then fit the experimental bulk modulus over part of the pressure range to a linear function of pressure.

$$B_f(p) = B_{0,f} + B_{1,f}p \quad (4)$$

from which the volume $V_f(p)$ of the fluid and the length $L(p)$ of the sample can then be computed

$$V_f(p) = V_{0,f}\left[1-\frac{1}{B_{1,f}}\ln\frac{B_{0,f}+B_{1,f}p}{B_{0,f}}\right] \quad (5)$$

$$L(p) = \frac{V_f(p)+V_{\mathrm{PE}}(p)}{D^2\pi/4} \quad (6)$$

where

$$V_{\mathrm{PE}}(p) = V_{0,\mathrm{PE}}\left[1-\frac{1}{B_{1,\mathrm{PE}}}\ln\frac{B_{0,\mathrm{PE}}+B_{1,\mathrm{PE}}p}{B_{0,\mathrm{PE}}}\right] \quad (7)$$

is the volume of the polyethylene sleeve. We combine eq (3) with eqs (5), (6), and (7) and rearrange to solve for h_0

$$h_0 = h(p) - L_0 + \frac{L_0}{D^2}\left[(D^2-d^2)\left(1-\frac{1}{B_{1,\mathrm{PE}}}\ln\frac{B_{0,\mathrm{PE}}+B_{1,\mathrm{PE}}p}{B_{0,\mathrm{PE}}}\right) + d^2\left(1-\frac{1}{B_{1,f}}\ln\frac{B_{0,f}+B_{1,f}p}{B_{0,f}}\right)\right] - \phi\bar{p}_r - \eta\bar{p}_r^2 - \gamma[1-e^{-\epsilon\bar{p}_r}] - \beta_{\mathrm{cyl}}L_0 p. \quad (8)$$

Now h_0 can be extrapolated from any datum point p. This procedure is unsatisfactory, at least in the present case, because the bulk modulus of the very compressible liquids is not a linear function of pressure and furthermore because in many instances the lowest pressure point is at 2000 bar and the extrapolation is rather long.

A low-pressure dilatometer was therefore constructed and measurements of $B_{0,f}$ were made to aid in the determination of h_0.

3. Low-Pressure Dilatometer

A simple low-pressure dilatometer was constructed to measure the isothermal compressibility of liquids at atmospheric pressure. The pressure vessel is shown in figure 2. The lower half is a 5-in o.d. stainless steel tube brazed to a brass bottom plate and closed at its upper end by a brass midplate sealed with an O-ring and held to the bottom plate by six long bolts. The midplate is drilled and tapped to receive a platinum resistance thermometer and a flare fitting for the pressure tap. In addition the midplate holds a transparent plastic tube into which the capillary of the dilatometer protrudes. This plastic tube is sealed by O-rings and held to the midplate by bolts from a top closure.

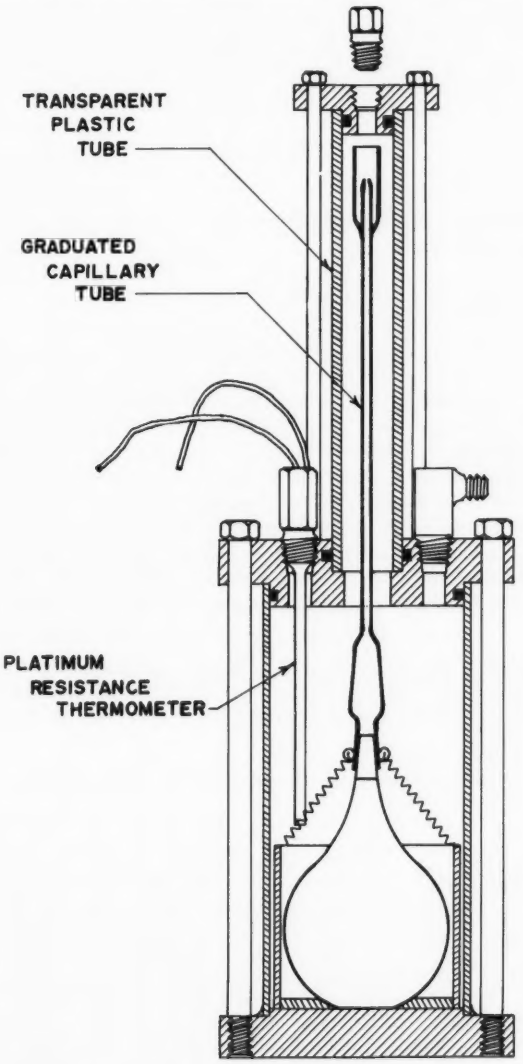

FIGURE 2. *Low-pressure dilatometer.*

The dilatometer is made from a 500-ml round-bottom flask sealed to the male portion of a ground-glass taper joint. A 0.2-ml graduated pipet was sealed to the female portion of the ground-glass taper joint. The upper end of the pipet has an open cup sealed around it to aid in the final filling. When assembled the readable portion of the scale on the pipet covers approximately 0.17 ml, graduated in 0.001 ml. The flask is nested in a perforated brass can with springs attached to the rim which hook over a clamp around the ground-glass joint of the pipet to hold the joint together. The can also serves to locate the dilatometer in the pressure vessel.

The base plate of the pressure vessel was maintained slightly above room temperature to permit thermostatic control of the temperature. The same fluid used in the dilatometer was also used as a bath fluid to fill the pressure vessel around the dilatometer to about one inch below the midplate. The same fluid was chosen to decrease evaporation from the open capillary and to cause similar changes in temperature due to change in pressure. Nitrogen was used above the liquid as the pressure fluid.

The volume of the dilatometer was determined to within 0.2 percent by the weight of water contained in it. The capillary scale was checked with a weighed slug of mercury and was found to be within 0.2 percent of the capillary volume and uniform to within 0.2 division. The pressure was measured with a calibrated bourdon tube gage. The temperature of the liquid surrounding the dilatometer within the pressure vessel was measured with a platinum resistance thermometer.

After filling the apparatus with a sample of fluid, the position of the meniscus in the capillary was read at various temperatures and at pressures between 1 and 5 bars.

The data were fitted to eq (9) by OMNITAB FIT for V_{f0}, K_f, α_f.

$$V_{D0} + V_{D0}\alpha_g(t - t_0) - V_{D0}K_g(P - P_0) + V_c = V_{f0} - V_{f0}K_f(P - P_0) + V_{f0}\alpha_f(t - t_0) \qquad (9)$$

where

V_{D0} is the volume of the dilatometer at P_0 and t_0,
α_g is the volumetric thermal coefficient of the glass,
K_g is the compressibility of the glass,
V_c is the reading of the fluid level in the capillary at P, t,
P is the pressure,
t is the temperature,
P_0 is standard atmospheric pressure,
t_0 is an assigned reference temperature near room temperature,
V_{f0} is the volume of fluid at P_0, t_0,
K_f is the compressibility of the fluid, and
α_f is the volumetric thermal coefficient of the fluid.

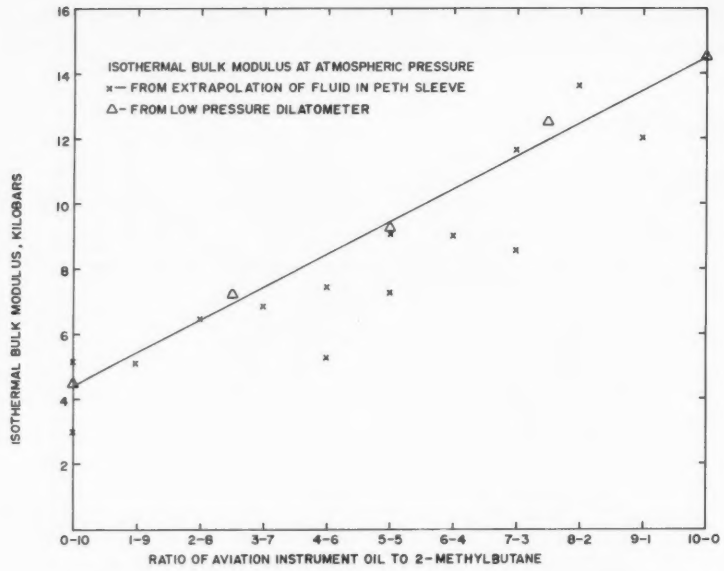

FIGURE 3. *Isothermal bulk modulus of mixtures of 2-methylbutane (i-pentane) and aviation instrument oil at atmospheric pressure.*

The estimated systematic uncertainties in the measurements of K_f are 0.2 percent due to V_{D0}; 1 percent for α_g and K_g; 0.3 percent for p; 0.2 percent for V_c; and 3 percent for t. The largest uncertainty, the 3 percent for t, results from an estimated uncertainty of 0.02 °C in the measurement of the equilibrium temperature. While this method of measuring the isothermal compressibility at atmospheric pressure gives results good only to about 3 percent, this is sufficient for our present use. The results for 2-methylbutane, aviation instrument oil, and 50/50, 75/25, and 25/75 mixtures of the two are shown in figure 3 by (Δ) as the isothermal bulk modulus at atmospheric pressure ($B^L_{0,f}$).

4. Results

Evaluation of the experimental data requires the determination of h_0 from eq (8). For this purpose and in spite of the slight nonlinearity, the bulk modulus values

$$B_f(p_m)=\frac{(p_{n+1}-p_n)V_{f0}}{V_f(p_n)-V_f(p_{n+1})} \tag{10}$$

with

$$p_m=\frac{p_n+p_{n+1}}{2}$$

were fitted to

$$B_f(p)=B_{0,f}+B_{1,f}p$$

for the first six non-zero pressures (approximately 1 to 10 kbar) for each fluid sample. The resulting $B_{0,f}$ are plotted (x) in figure 3 and both coefficients are listed in table 1. A considerable improvement can be made, if $B_{0,f}$ is set equal to $B^L_{0,f}$, the zero-pressure bulk modulus obtained from the low-pressure dilatometer measurements. A straight line is fitted to the same $B_f(p_m)$ as used above and forced through $B^L_{0,f}$. The $B^L_{0,f}$ are also plotted (Δ) in figure 3 and the coefficients $B^L_{0,f}$ and $B^F_{1,f}$ are listed in table 1. The values of $B^L_{0,f}$ and $B^F_{1,f}$ for each mixture were used to obtain an h_0 from eq (8) by averaging the values of h_0 from the first six non-zero pressure points for each mixture.

TABLE 1. *Density at atmospheric pressure and coefficients of bulk modulus of mixtures of aviation instrument oil and 2-methylbutane*

Ratio of aviation instrument oil to 2-methylbutane	ρ_0	$B_{0,f}$	$B_{1,f}$	$B^L_{0,f}$	$B^F_{1,f}$
	g/cm³	*kbar*		*kbar*	
0–10	0.615	2.99	11.54	4.5	11.27
0–10	.615	5.13	11.14	4.5	11.26
1–9	.651	5.07	11.24	5.5	11.16
2–8	.678	6.43	10.96	6.5	10.95
3–7	.705	6.82	10.99	7.5	10.87
4–6	.730	7.43	11.18	8.5	10.99
5–5	.752	7.25	11.69	9.5	11.30
5–5	.752	9.09	11.75	9.5	11.68
6–4	.781	8.98	11.37	10.5	11.11
7–3	.807	11.68	11.36	11.5	11.39
8–2	.827	13.61	11.21	12.5	11.40
9–1	.851	12.00	11.14	13.5	10.88
10–0	.879	10.41	12.10	14.5	11.28

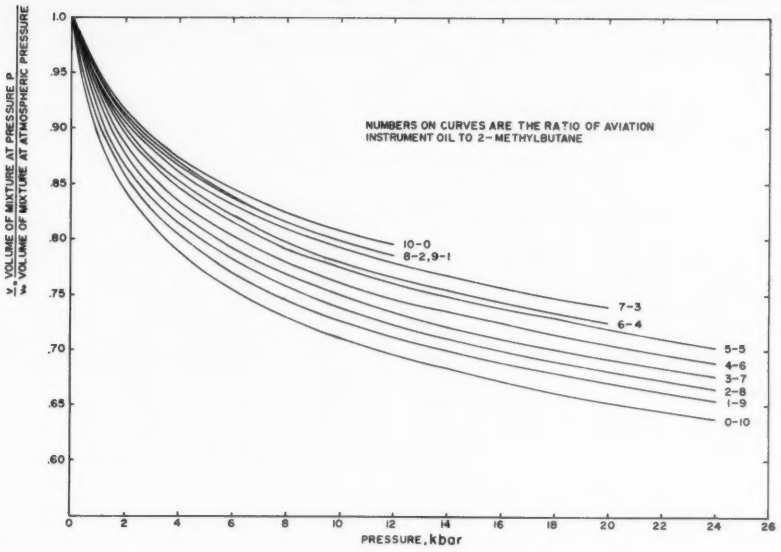

FIGURE 4. *Ratio of volume at pressure to volume at atmospheric pressure as a function of mixture and pressure.*

These values of h_0 are used in eq (3) for $L(p)$. $L(p)$ is used in eq (2) to determine $V_f(p)$. Figure 4 shows $V_f(p)/V_{f0}$ (or ρ_0/ρ) for each mixture. The values for $V_f(p)/V_{f0}$ are given in table 2.

Table 3 shows the values of the isothermal bulk modulus for each mixture at various pressures. The values at atmospheric pressure are obtained from a linear fit to the values of the low-pressure dilatometric data. All other values are from linear interpolation between nearest experimental values. The tabulated data were fitted to $B_T^*(m,p) = A + Bm + Cm^2 + Dp + Emp + Fm^2p + Gp^2 + Hmp^2 + Im^2p^2$. The variable m is the fraction of aviation instrument oil in the mixture of the oil and 2-methylbutane and p is the pressure. The results indicated that an acceptable fit for the accuracy of this data could be obtained with just the terms A, Bm, Dp, Emp, and Gp^2. A fit was made for these variables and the result is:

$$B_T^*(m,p) = 4.542 + 9.568\,m + 8.735\,p + 1.471\,mp - .06348\,p^2 \qquad (11)$$

for B_T^* and p in kilobars. These results are shown in figure 5.

The adiabatic bulk modulus for 2-methylbutane was computed from ultrasonic measurements of the time of flight and the dilatometric measurements of density and length of sample. The ratio of the adiabatic bulk modulus (B_S) to the isothermal bulk modulus (B_T^*)

TABLE 2. *Ratio of* V/V_0

Pressure in kilobars	Ratio of aviation instrument oil to 2-methylbutane										
	0–10	1–9	2–8	3–7	4–6	5–5	6–4	7–3	8–2	9–1	10–0
0.5	0.930	0.940	0.954	0.958	0.962	0.966	0.966	0.970	0.971	0.974	0.976
1	.893	.903	.911	.920	.926	.934	.938	.941	.944	.949	.952
2	.843	.856	.866	.876	.885	.893	.898	.905	.909	.912	.919
3	.811	.825	.836	.846	.856	.866	.871	.879	.885	.887	.893
4	.788	.803	.814	.824	.835	.846	.851	.860	.866	.868	.874
6	.754	.770	.781	.792	.803	.814	.821	.831	.838	.838	.845
8	.730	.746	.757	.768	.779	.791	.798	.809	.816	.816	.824
10	.711	.727	.738	.749	.761	.774	.780	.792	.799	.798	.807
12	.696	.712	.722	.734	.747	.760	.766	.779	.786	.784	.796
14	.684	.700	.710	.721	.734	.750	.754	.767			
16	.672	.689	.700	.710	.724	.737	.743	.756			
18	.662	.679	.690	.701	.714	.728	.733	.747			
20	.653	.670	.681	.692	.705	.719	.724	.738			
22	.645	.662	.672	.684	.697	.711					
24	.638	.654	.665	.676	.689	.703					

as a function of pressure for 2-methylbutane is shown in figure 6. The value 1.33 plotted at atmospheric pressure is the ratio of B_S/B_T^* obtained from data from the International Critical Tables [6].

TABLE 3. *Isothermal bulk modulus* (−V dp/dV) *in kilobars*

Pressure in kilobars	Ratio of aviation instrument oil to 2-methylbutane										
	0–10	1–9	2–8	3–7	4–6	5–5	6–4	7–3	8–2	9–1	10–0
0	4.5	5.5	6.5	7.5	8.5	9.5	10.5	11.5	12.5	13.5	14.5
2	22.2	23.8	24.4	25.8	26.0	27.5	28.6	30.9	33.8	31.2	32.3
4	37.9	40.1	40.6	41.6	43.1	45.3	46.4	49.6	50.4	48.7	50.2
6	54.3	56.1	58.2	59.1	60.0	62.2	63.0	66.4	69.0	67.6	69.1
8	70.0	70.7	70.5	72.1	75.6	80.3	79.8	82.8	83.8	81.8	88.5
10	88.9	86.6	86.1	90.9	97.9	98.9	103.8	114.1	112.5	103.6	118.6
12	102.1	112.0	106.5	106.0	113.3	122.3	115.5	124.6	133.3	127.2	162.4
14	113.2	122.8	125.1	124.4	127.3	129.8	125.4	133.7			
16	122.2	130.6	140.6	139.1	141.2	149.3	147.7	148.7			
18	138.2	144.6	147.5	149.7	153.5	157.2	157.8	164.4			
20	153.8	149.3	158.9	173.6	165.5	172.3	165.5	173.0			

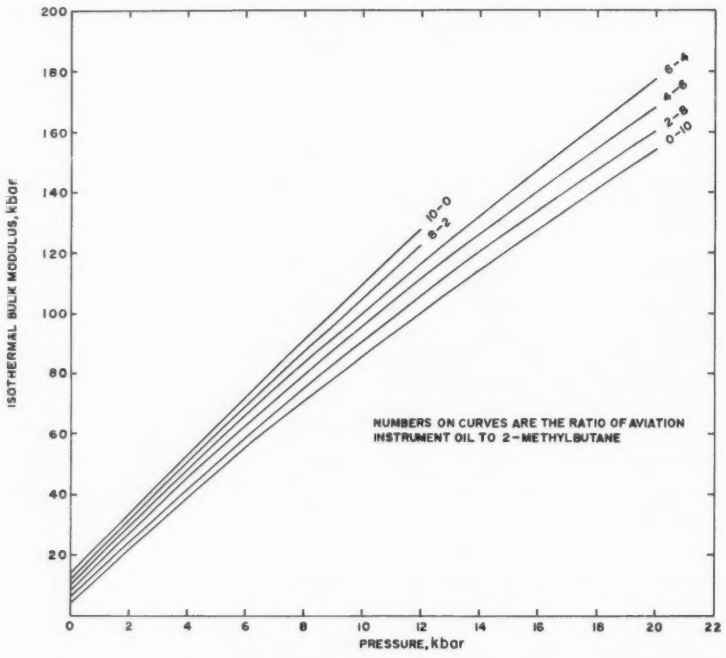

FIGURE 5. *Smoothed values of isothermal bulk modulus* (B_T^*=−Vdp/dV) *as a function of mixture and pressure.*

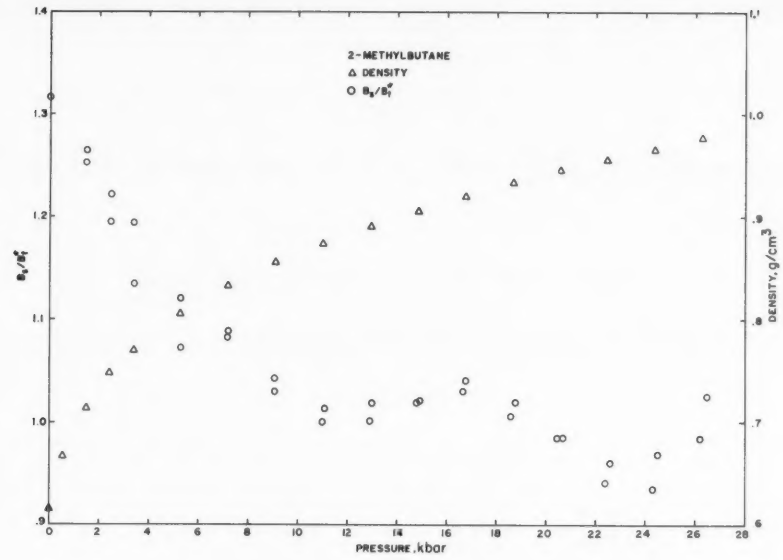

FIGURE 6. *Density and the ratio of adiabatic bulk modulus to isothermal bulk modulus of 2-methylbutane as a function of pressure.*

5. Conclusions

The use of a low-pressure dilatometer for measurement of isothermal bulk modulus of various liquids has proved useful in fitting data obtained in our high-pressure piston and die with polyethylene fluid container. This has resulted in more usable values for the bulk modulus and relative volumes of the liquids at high pressure.

6. References

[1] Jayaraman, A., et al. Rev. Sci. Instr. **38,** 44 (1967).

[2] Zeto, R. J., and Van Fleet, H. B., J. Appl. Phys. **40,** 2227 (1969).

[3] Bridgman, P. W., Proc. Am. Acad. Arts Sci. **66,** 199–200 (1931).

[4] Heydemann, P., and Houck, J. C., J. Appl. Phys. **40,** 1609 (1969).

[5] Heydemann, P., and Houck, J. C., Nat. Bur. Stand. (U.S.), Spec. Publ. 326. Proc. Symp. Accurate Characterization of the High-Pressure Environment, Gaithersburg, Maryland, 1968.

[6] International Critical Tables, Edward W. Washburn (McGraw-Hill Book Co., New York, Vol. III, page 39, 1928).

(Paper 75A2–655)

JOURNAL OF RESEARCH of the National Bureau of Standards—A. Physics and Chemistry
Vol. 75A, No. 2, March–April 1971

Crystal Structure of $Ca_2Na_2(CO_3)_3$ (Shortite)

B. Dickens, A. Hyman,* and W. E. Brown**

Institute for Materials Research, National Bureau of Standards, Washington, D.C. 20234

(December 18, 1970)

$Ca_2Na_2(CO_3)_3$ crystallizes in the orthorhombic unit cell $a=4.947(1)$ Å, $b=11.032(2)$ Å, and $c=7.108(1)$ Å at 25 °C with two formula weights in space-group Amm2. The structure has been redetermined, corrected, and refined to $R_w=0.025$, $R=0.020$ using 684 "observed" x-ray reflections from a single crystal. Corrections were made for absorption and isotropic extinction. In the extinction refinements, r refined to 0.00017(1) cm. The structure consists of Ca_2NaCO_3 layers interleaved with $Na(CO_3)_2$ layers. The Ca ion is coordinated strongly to nine oxygens, including three CO_3 edges, with Ca. . . O distances varying from 2.401(2) Å to 2.576(2) Å. One Na ion is coordinated strongly to eight oxygens, including two CO_3 edges, with Na. . . O distances from 2.429(2) Å to 2.605(1) Å. The other Na ion is coordinated strongly to six oxygens, including one CO_3 edge, at 2.296(1) Å to 2.414 Å, and weakly to a seventh at 3.050(3) Å. One CO_3 group is coordinated to seven cations, the other is coordinated to eight. The CO_3 groups have seemingly maximized their edge sharing with Ca ions rather than Na ions.

Key words: Calcium sodium carbonate; crystal structure; shortite; single-crystal x-ray diffraction.

1. Introduction

As part of a program of studies [1, 2][1] to obtain precise structural parameters on calcium carbonates, calcium carbonate hydrates, calcium phosphates, and related compounds, we have reinvestigated the crystal structure of $Ca_2Na_2(CO_3)_3$, which exists in nature as the mineral shortite. The structural features in these compounds are important in the consideration of possible epitaxial, syntaxial, and substitutional solid solution relationships in the major inorganic phases found *in vivo*.

Shortite was first found [3] in a matrix of montmorillonite clay which also contains pyrite (FeS_2), calcite ($CaCO_3$), and a carbonate of magnesium in crystals which were too small to be identified. Massive deposits of the commercially important mineral trona ($Na_2CO_3 \cdot NaHCO_3 \cdot H_2O$) are also found in the vicinity. A crystal structure for shortite has been reported by Wickman [4], who suggested atomic positions on the basis of refractive indices, spatial considerations, and the intensities of the $0kl$ reflections. We found this structure to contain one incorrect feature. The corrected structure of shortite is reported here.

2. Data Collection and Structure Refinement

The crystal used in the data collection is an approximate sphere, radius 0.112(4) mm, ground from a shortite fragment from mineral sample 105807, National Museum of Natural History, Smithsonian Institution, Washington, D.C. (sample supplied by J. S. White, Jr.). The sphere was mounted on the goniometer head in our usual way [2].

formula (ideal): $Ca_2Na_2(CO_3)_3$
cell: orthorhombic
$a=4.947(1)$ Å
$b=11.032(2)$ Å
$c=7.108(1)$ Å
volume = 387.9 Å^3
space-group Amm2;
cell contents $2[Ca_2Na_2(CO_3)_3]$
reciprocal lattice extinctions: $k+l=2n+1$ for hkl;
calculated density 2.620 g · cm^{-3};
observed density 2.629 g · cm^{-3} [3].

The procedure given in reference [2] was followed in the collection and processing of data with the following exceptions. The θ–2θ scans were carried out at 2°/min. Each background was counted for 20 s. 1659 reflections were collected from the hkl and $\bar{h}kl$ octants and were merged into a unique set of 711, of which 684 are "observed" and 27 are "unobserved." The R factor between observed equivalent reflections was 0.01. No absorption corrections were made because the maximum error in an intensity due to absorption is 0.8 percent. For $Ca_2Na_2(CO_3)_3$, μ(Mo) = 15.7 cm^{-1}. The Picker[2] hardware dropped the least significant

*Department of Chemistry, University of Maryland Baltimore County, Baltimore, Md.
**Director, American Dental Association Research Program, National Bureau of Standards, Washington, D.C. 20234.
[1] Figures in brackets indicate the literature references at the end of this paper.

[2] Certain commercial equipment, instruments, or materials are identified in this paper in order to specify the experimental procedure adequately. In no case does such identification imply recommendation or endorsement by the National Bureau of Standards, nor does it imply that the material or equipment identified is necessarily the best available for the purpose.

413-992 O - 71 - 3

digit during the data collection so that the standard deviations from counting statistics, and consequently our assessment of whether a given reflection is observed or unobserved, is only marginally correct. This affects very few reflections in the present case because the sample scattered strongly and nearly all reflections were unequivocally "observed" (modified hardware was used in later investigations). $\sigma(F)$ was defined as $F/10$ for $F < 10$; 1 for $10 < F < 43$; and $F/43$ for $F > 43$, where F_{max} was 211; weights in the least-squares refinements were $1/\sigma^2$. Wickman's structure [4] for $Ca_2Na_2(CO_3)_3$ would not refine to a residual, R_w, below 0.3. Examination of the Patterson function and an F_0 electron density Fourier synthesis phased from structure factor calculations using the positions of the Ca and Na ions suggested new positions for the C(1) and O(1) atoms. This structure was refined isotropically to $R_w = 0.056$, $R = 0.050$, and anisotropically to $R_w = 0.030$, $R = 0.023$ and then to $R_w = 0.025$, $R = 0.020$ with refinement on the isotropic extinction parameter, r, in addition to the previously varied parameters. The least-squares program RFINE written by Finger [5] was used. Only observed reflections were used in these refinements. The scattering factors for the neutral atoms were taken from Cromer and Mann [6]. No corrections for anomalous dispersion were made. The final value of r is 0.00017(1) cm where $F^2 = F_{unc}^2 \ (1 + \beta r |F_{unc}|^2)^{1/2}$ and F_{unc} is the structure factor uncorrected for extinction. The notation is that of Zachariasen [7]; here r may be related to the average domain size if the crystal is of type II where the extinction is assumed to be governed by spherical domains. The z coordinate of Ca was set equal to zero to define the origin along c. In the final cycle, the average shift/error was 0.01 and the standard deviation of an observation of unit weight,

$$[\Sigma W(F_0 - F_c)^2/(711-50)]^{1/2},$$

was 0.45.

The highest peaks in an electron density difference synthesis calculated at $R = 0.03$ corresponded to about 0.1 of an electron. The largest correlation coefficients are 0.42–0.44 between the scale factor and the B_{11}, B_{22}, and B_{33} temperature factors of Ca and 0.64 between the extinction parameter and the scale factor. All other correlation coefficients are less than 0.28.

The atomic parameters are given in table 1. All atoms but O(2) lie in special positions; the Wyckoff symbol and symmetry of these positions are given in table 1. The observed and calculated structure factors, uncorrected for extinction, are given in table 2.

3. Description of the Structure

The structure of $Ca_2Na_2(CO_3)_3$ is shown in figures 1 and 2. There are Ca_2NaCO_3 layers at $x = 0.5$ and $Na(CO_3)_2$ layers at $x = 0$. The CO_3 group containing C(2), O(3), O(4), and O(4′) lies on the mirror at $x = 0.5$ and is a member simultaneously of three cation-anion chains in which cations are coordinated to edges and opposite apexes of the CO_3 group. One $CaCO_3$ chain runs parallel to [011], one runs parallel to $[0\bar{1}1]$, and one $NaCO_3$ chain runs parallel to [001]. Similar cation-anion chains are present in the barytocalcite phase of $BaCa(CO_3)_2$ [8]. The bonding of the apex of the CO_3 group in the $NaCO_3$ chain to Na is weak, however. The CO_3 group containing C(1), O(1), O(2), and O(2′), which is on the mirror at $x = 0$ and has its plane parallel to (011) or $(0\bar{1}1)$, forms $NaCO_3$ chains like those cation-anion chains at $x = 0.5$. The two oxygens O(2) and O(2′), which lie above and below the mirror, provide bonding with cations in neighboring $Ca_2Na(CO_3)$ layers. Each Na at $x = 0$ is common to two chains. The CO_3 groups have seemingly oriented themselves to maximize edge coordination to Ca; each CO_3 group is bonded edge-wise to two Ca ions and one Na ion. Preferential edge coordination of CO_3 to Ca is in accord with Ca exerting the largest electrostatic attraction on the CO_3 group and is consistent with the Ca coordinations in $CaCO_3 \cdot 6H_2O$ [1], $CaNa_2(CO_3)_2 \cdot 5H_2O$ [9], and $CaNa_2(CO_3)_2 \cdot 2H_2O$ [9].

There is a void in the structure centered at about 0, 0.5, 0.8 (figs. 1 and 2). If the ionic radius of the oxygen in the CO_3 groups is assumed to be 1.4 Å, this void is about 2.2–2.5 Å in diameter. Because it has both cations and anions in its surface, it is unlikely that it would be occupied, except perhaps by an inert gas atom.

TABLE 1. *Atomic parameters of* $Ca_2Na_2(CO_3)_3$

Atoms	(a)	x	y	z	B_{11}^*	B_{22}	B_{33}	B_{12}	B_{13}	B_{23}
Ca	*e*, *m*, 4	0.5	0.21659(4)	0.0	0.65(1)	0.48(1)	0.58(1)	.....	.....	−0.01(1)
Na(1)	*a*, *mm*, 2	0.0	0.0	0.9263(3)	1.27(6)	0.97(5)	1.54(6)	.....	.....	.....
Na(2)	*b*, *mm*, 2	0.5	0.0	0.6122(3)	1.15(5)	0.69(5)	1.15(5)	.....	.....	.....
C(1)	*d*, *m*, 4	0.0	0.2961(2)	0.1697(3)	0.57(6)	0.84(7)	0.64(5)	.....	.....	−0.04(5)
O(1)	*d*, *m*, 4	0.0	0.1985(2)	0.0742(3)	1.08(6)	1.35(7)	1.44(7)	.....	.....	−0.81(6)
O(2)	*f*, 1, 8	0.2261(3)	0.3456(1)	0.2152(2)	0.59(4)	1.02(4)	1.08(4)	−0.19(3)	−0.04(3)	−0.02(3)
C(2)	*b*, *mm*, 2	0.5	0.0	0.2253(5)	1.1(1)	0.58(8)	0.64(9)	.....	.....	.....
O(3)	*b*, *mm*, 2	0.5	0.0	0.0415(4)	1.7(1)	0.60(7)	0.61(7)	.....	.....	.....
O(4)	*e*, *m*, 4	0.5	0.1013(2)	0.3111(3)	2.10(7)	0.57(5)	0.99(6)	.....	.....	−0.23(5)

Figures in parentheses are standard errors in last significant figure quoted, and were computed in the final cycle of full-matrix least-squares refinement.

[a] Wyckoff symbol, site symmetry, and multiplicity of site in space-group Amm2.

*Thermal parameters have the form $\exp(-1/4\ (a^{*2}B_{11}h^2 + b^{*2}B_{22}k^2 + c^{*2}B_{33}l^2 + 2a^*b^*B_{12}hk + 2a^*c^*B_{13}hl + 2b^*c^*B_{13}kl))$.

TABLE 2. *Observed and calculated structure factors for* $Ca_2Na_2(CO_3)_3$ *(shortite)*

Columns are *l*, $10F_o$, $10F_c$ and phase in millicycles. "Unobserved" reflections are marked by *. The F_c values do not include corrections for extinction. F_o and F_c are on an absolute scale.

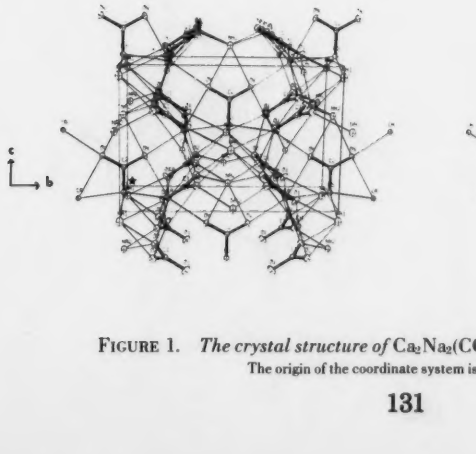

FIGURE 1. *The crystal structure of* $Ca_2Na_2(CO_3)_3$, *shortite, viewed along* a.
The origin of the coordinate system is marked by *.

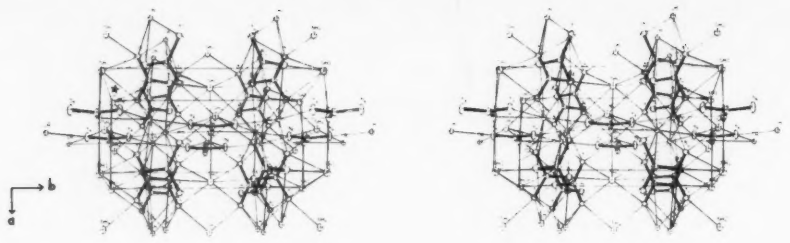

FIGURE 2. *As in figure 1 but viewed along* c.

3.1. The Calcium Ion Environment

The Ca ion lies on a mirror plane at $x = 0.5$. Its environment is shown in figure 3 and summarized in table 3. The coordination contains three CO_3 edges, $O(1^I, 2^I)$, O(1, 2) and O(3, 4), and three CO_3 apexes, $O(2^{II})$, $O(2^{III})$ and $O(4^I)$. The Ca . . . O distances indicate strong ionic bonding from Ca to all these oxygen atoms and are in the normal range. Strong coordination to nine neighboring oxygens is rare for Ca and is possible here because of the small O . . . O separation (~ 2.2 Å) in the edge of the CO_3 group. A large coordination number for Ca is favored by the Ca . . . O interaction being the strongest electrostatic attraction in the crystal. The Ca ions are about 4 Å apart in the structure; the shortest Ca . . . Na distance, with associated weaker electrostatic repulsion than Ca . . . Ca, is about 3.5 Å.

TABLE 3. *The calcium environment in* $Ca_2Na_2(CO_3)_3$

Atoms	Distance
	Å
Ca, O(4)	2.401(2)
Ca, O(3)	2.411(1)
Ca, O(2, 2^I, 2^{II}, 2^{III})	2.508(1)
Ca, O(1, 1^I)	2.543(1)
Ca, O(4^I)	2.576(2)

In all tables of interatomic distances and angles, the quantities in parentheses are standard errors in the last significant figure and were computed from the standard errors in the atomic positional parameters and in the cell parameters. They include contributions from the variance co-variance matrix. The atom labels refer to atoms in figure 3.

3.2. The Na Ion Environments

There are two crystallographically distinct Na ions in the crystal structure. Na(2) and Ca lie in the same plane perpendicular to [100]. Na(1) lies halfway between the planes containing Na(2) and Ca. Both Na ions lie at the intersections of mirror planes.

Na(1) is coordinated (fig. 3 and table 4) to eight oxygen atoms, of which $O(2^{III}, 2^{IV})$ and $O(2^V, 2^{VI})$ are CO_3 edges. All the Na(1) . . . O distances are within the normal range and indicate strong ionic bonding. The coordination is similar to that of (i) the Ca ion $CaNa_2(CO_3)_2 \cdot 5H_2O$ [9], where the oxygens not in shared edges are in water molecules, and (ii) the Ca(1) ion in $Ca_5(PO_4)_2SiO_4$ [10].

TABLE 4. *The sodium environments in* $Ca_2Na_2(CO_3)_3$

Atoms	Distance
	Å
Na(1), O(1, 1^I)	2.429(2)
Na(1), O(2^{III}, 2^{IV}, 2^V, 2^{VI})	2.530(2)
Na(1), O(3, 3^I)	2.605(1)
Na(2), O(2^{II}, 2^{III}, 2^{VI}, 2^{VII})	2.296(1)
Na(2), O(4, 4^I)	2.414(3)
Na(2), O(3)	3.050(3)

The atom labels refer to atoms in figure 3.

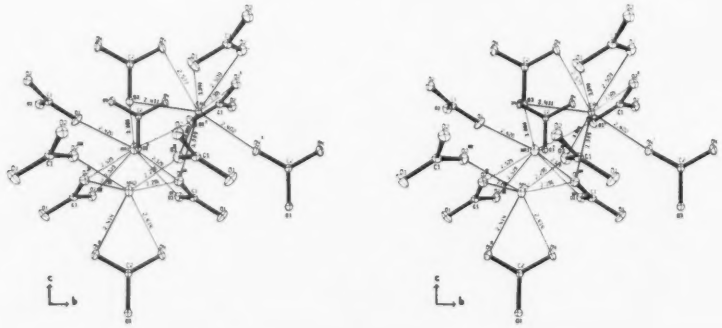

FIGURE 3. *The* Ca *and* Na *environments in* $Ca_2Na_2(CO_3)_3$.
The primes refer to atoms in tables 3 and 4.

Na(2) is bonded strongly to six oxygen atoms (table 4) essentially arranged in a square pyramid with a CO_3 shared edge O(4, 4^I) centered about the apex position (fig. 3). The environment of Na(2) is completed by O(3), which is, however, 3.050 Å away and thus bonded relatively weakly to Na(2). The geometry of strong coordination for Na(2) is like that of Na(2) in $Na_2CO_3 \cdot H_2O$ [11].

3.3 The CO_3 Groups and Their Environments

The dimensions of the CO_3 groups are given in table 5. The C(1) CO_3 group is nearly trigonal with an average C−O distance of 1.282 Å; the C(2) CO_3 group appears to be significantly non-trigonal, but with an average C−O distance of 1.283 Å. The average C−O distances compare well with 1.283(2) Å in calcite ($CaCO_3$) [12], 1.285 Å in aragonite ($CaCO_3$) [2], 1.286 Å in $Na_2CO_3 \cdot H_2O$ [11], 1.288 Å in $CaNa_2(CO_3)_2 \cdot 5H_2O$ [9], 1.286 Å in $CaNa_2(CO_3)_2 \cdot 2H_2O$ [9], and 1.286 Å in $CaCO_3 \cdot 6H_2O$ [1]. All these distances are uncorrected for thermal motion.

The environments of the CO_3 groups are shown in figure 4 and are summarized in table 5. All three edges of both CO_3 groups are coordinated, in both cases to two Ca ions and one Na ion in the same plane as the CO_3 group. All oxygen atoms are further coordinated: O(1) to Na(1) in the plane of the C(1) CO_3 group, O(2) to Ca and Na(2) both out of this plane, O(4) to Ca(1) in the plane of the C(2) CO_3 group, and O(3) to two Na(1) ions which are both out of this plane. Edge coordination of O(3, 4) and O(3, 4^I) to Ca is expected to decrease the O(3)−C(2)−O(4) and O(3)−C(2)−O(4^I) angles in accord with Pauling's rule because the O(4, 4^I) edge of the same CO_3 group is coordinated with weaker electrostatic force to Na(2). This is in accord with the observed O−C−O angles of 118.7(2)° for the Ca coordinated edges and 122.7(4)°, for the Na coordinated edge. Similar effects would be expected in the other CO_3 group, where O(1, 2) and O(1, 2^I) are coordinated to Ca and O(2, 2^I) is coordinated to Na. Here the angles, 119.6(1) for the Ca coordinated edges and 120.9(2)° for the Na coordinated edge are in the right directions from 120°, but are more nearly equal, which suggests that the effect is more complex than this simple reasoning. The average of the distances Ca . . . O(3) and Ca . . . O(4) is 2.493 Å; that of the Ca . . . O(1) and Ca . . . O(2) distances is 2.526 Å. The difference of 0.03 Å between these average values may account for part of the difference in angles of the CO_3 groups because O(3) and O(4) are bonded more strongly to Ca and the O(3), C(2), O(4) angle would then be expected to be decreased more than the O(1), C(1), O(2) angle.

In the absence of hydrogen bonding, the oxygens coordinated most strongly to cations may be expected to have the longest C−O bonds. This is qualitatively the case. Similar effects have been observed in $Na_2CO_3 \cdot H_2O$ [11], $CaNa_2(CO_3)_2 \cdot 5H_2O$ and $CaNa_2(CO_3)_2 \cdot 2H_2O$

TABLE 5. *The Carbonate Anions and Their Environments* $Ca_2Na_2(CO_3)_3$

Atoms	Distance, Å, or angle deg.
C(1), O(1)	1.273(3) Å
C(1), O(2, 2^I)	1.286(2)
O(1), O(2, 2^I)	2.211(2)
O(2), O(2^I)	2.238(2)
O(1), C(1), O(2, 2^I)	119.6(1)°
O(2), C(1), O(2^I)	120.9(2)
C(2), O(3)	1.306(4)Å
C(2), O(4, 4^I)	1.273(3)
C(3), O(4, 4^I)	2.218(3)
O(4), O(4^I)	2.235(4)
O(3), C(2), O(4, 4^I)	118.7(2)°
O(4), C(2), O(4^I)	122.7(3)
O(1), Na(1^I)	2.429(2) Å
O(1), Ca, Ca^I	2.543(1)
O(2), Na(2)	2.296(1)
O(2), Ca^{II}	2.508(1)
O(2), Ca^{III}	2.508(1)
O(2), Na(1)	2.530(2)
O(2), O(2^{III})	2.709(2)
O(3), Ca	2.411(1)
O(3), Ca^{IV}	2.411(1)
O(3), Na(1), Na(1^I)	2.605(1)
O(3), Na(2)	3.050(3)
O(4), Ca^{II}	2.401(2)
O(4), Na(2)	2.414(3)
O(4), Ca	2.576(2)

The atom labels refer to atoms in figure 4.

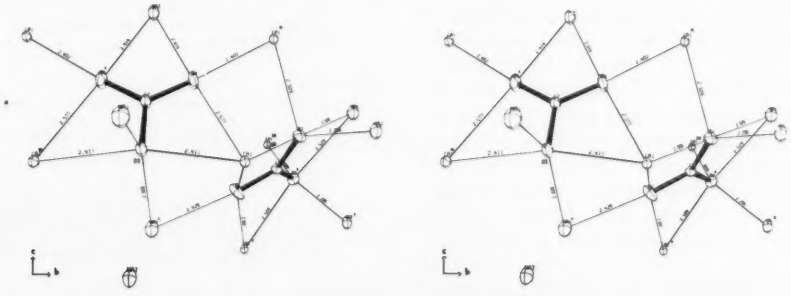

FIGURE 4. *The environments of the* CO_3 *groups in* $Ca_2Na_2(CO_3)_3$.
The primes refer to atoms in table 5.

[9] and in the PO_4 groups in $Ca_7Mg_9(Ca, Mg)_2(PO_4)_{12}$ [13]. In the C(1) CO_3 group in $Ca_2Na_2(CO_3)_3$, the bond distance C(1)–O(2) and the symmetrically equivalent distance C(1)–O(2^I) are slightly longer than C(1)–O(1). O(2) is coordinated to two Ca ions and two Na ions; O(1) is coordinated to one Ca ion and one Na ion. In the C(2) CO_3 group, C(2)–O(3) is appreciably longer than the two equivalent distances C(2)–O(4) and C(2)–O(4^I). O(3) is coordinated to two Ca ions and two Na ions; O(4) is coordinated to two Ca ions and one Na ion. The differences in the coordinations of O(3) and O(4) here do not appear large enough to explain the 0.035 Å difference in C–O bond lengths. The difference, 0.020 Å, in the bond lengths C(1)–O(2) and C(2)–O(3), may be partly explained by the fact that while the C(1) CO_3 group has two longer bonds, the C(2) CO_3 group has only one, which may therefore be expected to have approximately twice the extension due to the cation field that the C(1)–O(2) bonds have.

The C(1) atom in the C(1) CO_3 group is 0.012(3) Å out of the plane defined by the O(1), O(2), and O(2^I) atoms. This may be a result of perturbation of the sp^2 hybridization of the oxygen atoms by neighboring cations. The C(2) CO_3 group is planar by symmetry.

4. Discussion

The positions given by Wickman, (0.0, 0.226, 0.743) for C(1), (0.0, 0.325, 0.850) for O(1), and (0.230, 0.177, 0.690) for O(2), which are 0.57, 1.98, and 0.31 Å, respectively, from the positions given here, show that in his structure the C(1)O_3 group has been reflected along c through the plane $z=0.75$, so that O(1) then juts out into the void instead of being on the void surface. The interatomic distances are reasonable in Wickman's structure and the O . . . O repulsions are therefore approximately the same in the two models. In the structure reported here, however, O(1) is able to form stronger bonds to the two Ca ions above and below it along a, and to Na(1) in the same plane parallel to (100); this is probably the factor governing the orientation of the CO_3 group. The calculation of refractive indices in the way originally given by Bragg [14] assumes that only oxygen atoms have optical anisotropy and ignores all interatomic interactions. Thus, Wickman, following this procedure, was able to obtain qualitative agreement between observed and calculated values using a model in which the orientation of the C(1) CO_3 group relative to the (001) plane was $\sim 35°$ instead of $-31° 42'$. The average orientations of C(1) CO_3 groups in the unit cell are about the same for the two models when one takes into account the symmetry operations. This agreement can be seen from table 6, which compares the observed indices with the values calculated for the two models using Bragg's procedure. A much more suitable test of these models, which would produce better quantitative agreement with the observed values, would require consideration of dipole-dipole coupling terms and optical anisotropy of all atoms, especially Na, rather than just oxygens [15, 16]. As a further refinement, the dependence of the atomic optical anisotropy on the environment should be incorporated.

TABLE 6. *Refractive indices for shortite*

Observed	Wickman's model	Here	Orientation
1.531	1.515	1.502	c
1.555	1.545	1.541	a
1.570	1.555	1.554	b

J. S. Bowen collected the diffractometer data; P. B. Kingsbury used the ORTEP program of C. K. Johnson, Oak Ridge National Laboratory, to draw the figures. This investigation was supported in part by research grant DE-00572 to the American Dental Association from the National Institute of Dental Research and is part of the dental research program conducted by the National Bureau of Standards, in cooperation with the American Dental Association; the United States Army Medical Research and Development Command; the Dental Sciences Division of the School of Aerospace Medicine, USAF; the National Institute of Dental Research; and the Veterans Administration.

5. References

[1] Dickens, B., and Brown, W. E., The crystal structure of $CaCO_3 \cdot 6H_2O$ at ~ -120 °C, Inorg. Chem. **9**, 480–486 (1970).

[2] Dickens, B., and Bowen, J. S., Refinement of the crystal structure of aragonite ($CaCO_3$), J. Res. Nat. Bur. Stand. (U.S.) (in press).

[3] Fahey, J. J., Shortite, a new carbonate of sodium and calcium, Am. Min. **24**, 514–518 (1939).

[4] Wickman, F. E., The crystal structure of shortite, $Ca_2Na_2(CO_3)_3$, Arkiv for Mineral. Geol. **1**, 95–101 (1949).

[5] Finger, L. W., Determination of cation distribution by least-squares refinement of single-crystal X-ray data, Carnegie Institute of Washington Year Book **67**, 216–217 (1969).

[6] Cromer, D. T., and Mann, J. B., X-ray scattering factors computed from numerical Hartree Fock wave functions, Acta Cryst. **A24**, 321–324 (1968).

[7] Zachariasen, W. H., A general theory of X-ray diffraction in crystals, Acta Cryst. **23**, 558–564 (1967).

[8] Dickens, B., and Bowen, J. S., A refinement of the crystal structure of $BaCa(CO_3)_2$ (barytocalcite). J. Res. Nat. Bur. Stand. (U.S.) (in press).

[9] Dickens, B., and Brown, W. E., The crystal structures of $CaNa_2(CO_3)_2 \cdot 5H_2O$, synthetic gaylussite, and $CaNa_2(CO_3)_2 \cdot 2H_2O$, synthetic pirssonite, Inorg. Chem. **8**, 2093–2103 (1969).

[10] Dickens, B., and Brown, W. E., The crystal structure of $Ca_5(PO_4)_2SiO_4$ (silico-carnotite), Tschermaks Mineral. und Petrog. Mitteilungen (in press).

[11] Dickens, B., Mauer, F. A., and Brown, W. E., A refinement of the crystal structure of $Na_2CO_3 \cdot H_2O$, J. Res. Nat. Bur. Stand. (U.S.), **74A**, (Phys. and Chem.), 319–324 (1970).

[12] Chessin, H., Hamilton, W. C., and Post, B., Position and thermal parameters of oxygen atoms in calcite, Acta Cryst. **18**, 689–693 (1965).

[13] Dickens, B., and Brown, W. E., The crystal structure of $Ca_7Mg_9(Ca, Mg)_2(PO_4)_{12}$, Tschermaks Mineral. und Petrog. Mitteilungen (in press).

[14] Bragg, W. L., The refractive indices of calcite and aragonite, Proc. Roy. Soc. **A105**, 370–386 (1924).

[15] Lawless, W. N., and Devries, R. C., Oxygen polarizability and point-dipole theory in the carbonate minerals, J. Phys. Chem. Solids **25**, 1119–1124 (1964).

[16] Davis, T. A., and Vedam, K., Variation of the refractive indices of calcite, with pressure to 7 Kbar, Phys. Stat. Solids **26**, 285–290 (1968).

(Paper 75A2–656)

JOURNAL OF RESEARCH of the National Bureau of Standards—A. Physics and Chemistry
Vol. 75A, No. 2, March–April 1971

Publications of the National Bureau of Standards*

Selected Abstracts

Berger, M. J., Seltzer, S. M., **Bremsstrahlung and photoneutrons from thick tungsten and tantalum targets,** *Phys. Rev. C,* **2,** *No. 2, 621–631 (August 1970).*

Key words: Bremsstrahlung; bremsstrahlung efficiency; Monte Carlo; photon neutron; radiation transport; thick targets.

Monte Carlo calculations have been made of electron-photon cascades in thick tungsten targets bombarded by electrons with energies up to 60 MeV. The following information has been obtained: (1) the bremsstrahlung efficiency, (2) the angular distribution of the emitted bremsstrahlung intensity, (3) the spectra of the bremsstrahlung emitted in various directions, (4) the transmission of primary and secondary electrons through the target, (5) energy deposition as function of the depth in the target, (6) the differential photon track-length distribution inside the target, and (7) the yield of photoneutrons. The paper also includes various comparisons with experimental data.

Block, S., Weir, C. E., Piermarini, G. J., **Polymorphism in benzene, napthalene, and anthracene at high pressure,** *Science* **169,** *586–587 (August 7, 1970).*

Key words: Anthracene; benzene; high-pressure; naphthalene; polymorphism.

High-pressure optical observations using a microscope with the diamond-anvil pressure cell have (1) confirmed that there is a transition in naphthalene and no triple point to 500° ± 15 °C, (2) shown that there is a corresponding high-pressure transition in anthracene and no triple point to 550° ± 15°, (3) shown that a second reversible high-pressure form of benzene exists with a triple point (liquid-II-III) at 590° ± 15° and approximately 40 kbars, and (4) demonstrated that, at approximately 500° for anthracene, 550° for naphthalene and 600° for benzene III, these materials transform irreversibly to deep reddish-orange colored products which have not yet been characterized.

Bowen, R. L., **Crystalline dimethacrylate monomers,** *J. Dental Res.* **49,** *No. 4, 810–815 (July–August 1970).*

Key words: Dimethacrylates; thermosetting monomers; ternary eutectic; urification methods; resins for composites; phthalate monomers; biomaterials.

Certain dimethacrylate monomers can be prepared and purified by recrystallization. Upon mixing, the crystals liquify by forming a ternary eutectic. The colorless oily liquid is suitable for use in composite formulations.

Ensign, T. C., Chang, Te-Tse, Kahn, A. H., **Hyperfine and nuclear quadrupole interactions in copper-doped TiO_2,** *Phys. Rev.* **188,** *No. 2, 703–709 (Dec. 10, 1969).*

Key words: Copper; EPR; *g*-factors; hyperfine interaction; quadrupole coupling; rutile; titanium dioxide.

Single crystals of TiO_2:Cu^{2+} have been investigated at 20 K using the technique of electron paramagnetic resonance. The major features of the EPR spectra can be attributed to divalent copper ($3d^9$) in substitutional (Ti^{4+}) sites. Information has been gained about both isotopes of copper and about the interactions which concern this ion. For the substitutional site the spin Hamiltonian parameters in the S = 1/2, I = 3/2 manifold are: $g_x = 2.109$, $g_y = 2.094$, $g_z = 2.346$, $A_x^{63} = +18.7 \times 10^{-4}$ cm^{-1}, $A_y^{63} = +27.2 \times 10^{-4}$ cm^{-1}, $A_z^{63} = -87.5 \times 10^{-4}$ cm^{-1}, $A_x^{65} = +18.8 \times 10^{-4}$ cm^{-1}, $A_y^{65} = +28.7 \times 10^{-4}$ cm^{-1}, $A_z^{65} = -93.7 \times 10^{-4}$ cm^{-1}, $P_x = -2.56 \times 10^{-4}$, $P_y = -2.37 \times 10^{-4}$, $P_z = +4.93 \times 10^{-4}$ cm^{-1}. The magnitudes and relative signs of these parameters have been determined experimentally while the absolute signs have been predicted theoretically from a model which gives a consistent picture of the ordering of the d^9 electronic states. In addition, the theoretical treatment gives a satisfactory estimate of P. Departure from tetragonality was taken into account. The covalency parameter α^2 which measures the fraction of the hole wave function on the Cu^{2+} is found to be 0.71, and κ, the factor giving rise to isotropic hyperfine structure, is found to be 0.31.

Ensign, T. C., Stokowski, S. E., **Shared holes trapped by charge defects in $SrTiO_3$,** *Phys. Rev. B,* **1,** *No. 6, 2799–2810 (March 15, 1970).*

Key words: Color centers; EPR; hole centers; optical absorption; shared holes; $SrTiO_3$.

Using the techniques of EPR and optical irradiation in conjunction with optical absorption measurements, we have gained useful information about the nature of some hole centers in $SrTiO_3$. Primarily we have investigated single crystals doped with aluminum at temperatures near 77 K. Two principal centers have been explored: (1) the Al-O^- center—a hole shared among the oxygens which surround Al^{3+}, and (2) the X-O^- center—a hole shared in a similar fashion, but more deeply trapped by a charge defect of unknown origin. The Al-O^- center arises after band gap irradiation and is characterized at 77 K by the following *g*-values and hyperfine constants: $g_{\|} = 2.0137$, $g_{\perp} = 2.0124$, $A_{\|} = 8.3 \times 10^{-4}$ cm^{-1}, and $A_{\perp} = 7.6 \times 10^{-4}$ cm^{-1}. The X-O^- center is present before optical irradiation. No hyperfine structure is observed, but the isotropic *g*-value is 2.0130 at all temperatures from 4.2 to 300 K. An 800 nm absorption band arising after band gap excitation has been correlated with the Al-O^- center. 430 and 600 nm absorption bands have been correlated with the absence of Fe^{3+} in the EPR spectrum, and a 500 nm band has also been observed. In addition, the role of iron in the photochronic processes of $SrTiO_3$ is presented. Finally, theoretical work utilizing the molecular orbital σ and π states in O_h symmetry has provided a firm basis for the sharing model. The experimental *g* values and hyperfine constants are discussed in light of this model and are found to be in good agreement.

Estin, A. J., Editor, **Precision measurement and calibration. Selected NBS Papers on electricity-radio frequency,** *Nat. Bur. Stand. (U.S.), Spec. Publ. 300, Vol. 4, 456 pages (June 1970) $5.50, SD Catalog No. C13.10:300/v.4.*

Key words: Admittance; antenna; attenuator; bolometer; calorimetry; horn; impedance; interferometry; measuring system; phase; power; radiometry; resonant cavity; voltage; waveform; waveguide junction.

This volume is one of an extended series which brings together some of the previously published papers, monographs, abstracts, and bibliographies by NBS authors dealing with the precision measurement of specific physical quantities and the calibration of the related metrology equipment. The contents have been selected as being useful to the standards laboratories of the United States in tracing to NBS standards the accuracies of measurement needed for research work, factory production, or field evaluation.

Volume 4 contains reprints through June 1967 on radio-frequency electrical measurements covering the following topics: Power, Sinusoidal Voltage and Current, Electromagnetic Fields and Antennas, Radar and Baseband Pulses, Noise, Attenuation and Phase, Impedance, Radio Frequency Materials, Quasi-optics and Millimeter Waves, and Applications to Measurement Systems.

Furcolow, W. H., Technical Standards Coordinator, **Mosaic-parquet hardwood slat flooring,** *Nat. Bur. Stand. (U.S.), Voluntary Prod. Stand. 27–70, 13 pages (Sept. 1970), 25 cents, SD Catalog No. C13.20/2:27–70.*

Key words: Flooring; hardwood flooring; mosaic-parquet flooring; slat flooring.

This Voluntary Product Standard covers requirements for grading, moisture content, dimensions, construction, and finish for mosaic-parquet hardwood slat flooring which is intended for use in residential, institutional, and commercial buildings. A method for marking and labeling to indicate compliance with the Standard is also provided. Manufacturers' recommendations on ordering and installation are included in an appendix. The Standard does not cover flooring squares or blocks which are fabricated from conventional tongue and groove type strips.

Goldstein, J. I., Henderson, E. P., Yakowitz, H., **Investigation of lunar metal particles** (*Proc. Apollo 11 Lunar Science Conf., January 1970, Houston, Texas*), *Geochim. Cosmochim. Acta* **1**, *499–512 (1970).*

Key words: Electron probe microanalysis; lunar samples; lunar simulation; lunar thermal history; meteorites; probe microanalysis; scanning electron microscopy.

Several metallic particles from lunar fine samples 84 and 85–17M and from breccia sample 46–18A were investigated by means of optical microscopy, scanning electron microscopy and electron probe microanalysis. These particles consisted of two large globules, metal spread on glassy spheres, splinters and metal in the foamy pumice-like fragments. The largest globule had a structure consisting of 40 μm Fe-Ni dendrites in a matrix of troilite. A high Ni rim was found at the troilite-dendrite interface. The dendrites showed typical Ni segregation, the composition at the outside being about 16 w/o Ni with 13 w/o Ni at the center. The troilite contained 0.1 to 1.5 w/o Ni and appears to be in dis-equilibrium. The rim contains 29 to 46 w/o Ni and about 0.3 w/o S. The rim is a γ phase in the Fe-Ni-S system and was created by the rejection of Ni from the troilite. We were able to synthesize this globule; the same structure was obtained. From this simulation, the cooling rate was determined as 2.5° C/sec. This globule probably was created by the impact of a chondrite on the moon.

A globule separated from the breccia rock apparently solidified quickly and then cooled slowly, the rock acting as a kind of crucible. This globule's metal regions contain 2 w/o Ni, 1 w/o P, 0.3 w/o Co, balance Fe. There are also phosphide eutectic regions containing fine intergrowths of kamacite, troilite and carbides. This particle shows a striking simularity to spheroids from the Canyon Diablo iron. The evidence indicates that this globule was probably created by the impact of an iron meteorite on the moon.

The analysis of the metal particles makes it clear that both meteoritic and lunar Fe-FeS intergrowth are present in the lunar fines. The lunar metal is similar to the meteoritic material in that it is surrounded by sulfide; both metal constituents are of comparable size, structure and Co content. The two types of material can be differentiated by the significant Ni and P content of the transformed original meteoritic material.

Holt, H. K., **Theory of gas lasers and its application to experiment,** *Phys. Rev. A*, **2**, *No. 1, 233–249 (July 1970).*

Key words: Collisions; gas laser; line widths; power output; theory; tuning curves.

The semi-classical theory of gas lasers has been reformulated using rate equations to describe the density matrix time behavior. The solution to these equations, in the form of a Fourier series, is applicable to arbitrarily high laser intensities. A calculation of the effect of phase-changing collisions is also included. The results are compared to experimental data taken with a He-Ne laser operating at a wavelength of 1.15 μm.

Klein, R., **A field emission study of carbon monoxide on h.c.p. metals rhenium and ruthenium,** *Surface Sci.* **20**, *No. 1, 1–17 (March 1970).*

Key words: Carbon monoxide; desorption; field emission; monoxide; rhenium, ruthenium, surface migration.

The surface migration, work function increments, and desorption of carbon monoxide on two h.c.p. metals, rhenium and ruthenium, were observed with field emission techniques. Carbon monoxide is weakly bound to ruthenium and more strongly bound to rhenium. For a complete monolayer, the work function increment is 1.3 eV for ruthenium and 0.8 for rhenium. Surface migration commences at a readily observable rate at about 125 K for ruthenium and shows both boundary and boundary free characteristics. Rhenium has an ill defined surface migration temperature region because the desorption precedes and overlaps it. Two well defined binding states for CO on rhenium are seen.

Ledbetter, H. M., Reed, R. P., **On the martensite crystallography of Fe-Ni alloys**, *Mater. Sci. Eng.* **5**, *No. 6, 341–349 (June 1970).*

Key words: Crystallographic theory; iron-nickel alloy; martensite.

For the first time lattice parameter data and habit plane measurements are available for an alloy system whose crystallographic features change continuously with composition. This information has been produced for the plate-like martensitic transformation in Fe-base alloys containing between 29 and 35 wt. % Ni. This paper presents a critical examination of the data from the viewpoint of the theories of martensite crystallography. It is found that the current theories cannot explain the variation of the habit plane with composition without invoking a varying δ (1.000 to 1.013), δ being an isotropic dilatation parameter. In addition to the habit plane, several quantities have been calculated as a function of composition: the volume change, the magnitude of the lattice invariant deformation, the magnitude and direction of the shape change, and the orientation relationship. The effects of errors in lattice parameter and of thermal expansion are considered.

Mann, W. B., Garfinkel, S. B., Editors, **Radioactivity calibration standards,** *Nat. Bur. Stand. (U.S.), Spec. Publ. 331, 120 pages (August 1970) $1.25, SD Catalog No. C13.10:331.*

Key words: Alpha-particle standards; calibration consistency; coincidence counting; decay-scheme effects; efficiency tracing; gamma-ray standards; international comparisons; liquid-scintillation counting; radionuclide half-lives; radionuclide standards.

Experimental procedures and methods used in nine international radioactivity standardization laboratories are described by eight authors. The possibility of attaining accuracies of the order of 0.01 percent are discussed. The desirability of carrying out consistency checks of gamma-ray standards with time, using a $4\pi\gamma$ ionization chamber is emphasized. The validity of radioactivity standards is examined. International comparisons organized by the Bureau International des Poids et Mesures are discussed. An analogue method of liquid-scintillation counting is described. Certain types of radioactivity standards are criticized. The fields of interest of the two Canadian laboratories are discussed. Details of the work in progress at the Boris Kidrič Institute and National Bureau of Standards are presented.

Milligan, D. E., Jacox, M. E., **Spectra of radicals in Physical Chemistry, 4,** *Chapter 5, 193–231 (Academic Press Inc., New York, N.Y., 1970).*

Key words: Electronic spectrum; flash photolysis; free radicals; matrix isolation; molecular orbitals; vibrational spectrum.

Problems arising in the direct spectroscopic detection of free radicals are surveyed. Apparatus used for the spectroscopic study of free radicals in the gas phase and trapped in inert solid matrices is

described. The advantage and limitations of flash photolysis and of matrix isolation studies for the production and detection of free radicals are considered. Examples of radicals studied by these techniques are cited, and data on the structure and chemical bonding of these species derived from the observed spectra are correlated with the predictions of simple molecular orbital theory.

Reimann, C. W., Santoro, A., Mighell, A. D., **The crystal molecular structure of hexapyrazolenickel(II) nitrate, $Ni(C_3H_4N_2)_6(NO_3)_2$,** *Acta Cryst.* **B26,** *Part 5, 521–526 (May 1970).*

Key words: Inorganic coordination complex; octahedral coordination; pyrazole; trigonal symmetry; x-ray structure determination.

The crystal structure of hexapyrazolenickel(II) nitrate, $Ni(C_3H_4N_2)_6(NO_3)_2$, was determined by single-crystal diffraction techniques. Crystals of $Ni(C_3H_4N_2)_6(NO_3)_2$ are trigonal with $a = 9.958$, $c = 7.278$Å, space group = $P\bar{3}$, $Z = 1$, $\rho_0 = 1.57$ g.cm^{-3}, $\rho_c = 1.57$ g.cm^{-3}. Three-dimensional counter data were collected (1115 reflections) and the structure was solved by an analysis of the Patterson map. The complex cation, $Ni(C_3H_4N_2)_6^{++}$, formed by the coordination of six planar pyrazole molecules to the nickel ion, has $\bar{3}$ point symmetry. The nickel ion lies at the center of a nearly regular octahedron of coordinated nitrogen atoms. These complex cations and nitrate anions are linked by hydrogen bonds between each pyrrole type nitrogen atom (N—H) in the pyrazole ring and an oxygen atom in the nitrate group. The final refinement by full matrix anisotropic least-squares analysis resulted in an R value of 0.053.

Ruff, A. W., Jr., **Measurement of stacking fault energy from dislocation interactions,** *Met. Trans.* **1,** *No. 9, 2391–2413 (Sept. 1970).*

Key words: Dislocations; dislocation nodes; dislocation ribbons; faulted dislocation dipoles; stacking fault energy; stacking fault tetrahedra.

The theories and methods applied to the determination of the stacking fault energy (γ) using techniques of direct observation of dislocation configurations are reviewed. The four principal methods, utilizing dislocation nodes, multiple ribbons, stacking fault tetrahedra, and faulted dipoles, are discussed in detail. Different theoretical treatments are compared wherever possible. Experimental procedures and quantitative measurement methods are reviewed. Detailed examples of the application of each method are given. For $\gamma/\mu b$ in the range of 2×10^{-4} to 5×10^{-3} (μ the shear modulus, b the Burgers vector), measurements on dislocation nodes or multiple ribbons in favorable cases should permit determinations of the stacking fault energy to a precision of 5 percent. For larger values of $\gamma/\mu b$ (up to 12×10^{-3}), measurements can be made on tetrahedra or faulted dipoles with less precision. Larger values of the stacking fault energy require high resolution studies of dislocations; these techniques are not yet well established. Possible sources of systematic bias are discussed. Two significant theoretical problems remain concerning the treatment of the dislocation core and the use of anisotropic elasticity. It is of prime importance to characterize as carefully as possible the materials studied if accurate results are desired.

Simson, B. G., Mandel, J., Brenner, F. C., **Research for a uniform quality grading system for tires. III. Breaking energy,** *Rubber Chem. Tech.* **43,** *No. 2, 356–369 (March 1970).*

Key words: Bias ply; breaking energy; passenger car; radial; tire strength; tires; winter.

A test procedure, designed to classify tires according to their average breaking energy has been applied to a sample of passenger car tires. Data are reported on 127 different tires of all grades and types over a range of sizes.
A scaling system is devised and applied to the data. It is found that the system leads to conclusions similar to those derived from the original data.

Ugiansky, G. M., Skolnick, L. P., Stiefel, S. W., **Directional effects in the stress corrosion cracking of an aluminum alloy,** *Corrosion* **25,** *No. 2, 77–86 (February 1969).*

Key words: Aluminum alloy; corrosion; directional effects; grain morphology; preferred orientation; stress corrosion.

Studies of the relative effects of grain morphology and preferred orientation on the directional susceptibility to intergranular stress corrosion cracking of a 7075–T651 aluminum alloy plate have been conducted. The role of grain morphology was found to be of paramount importance in controlling crack propagation. It was found that a slow rate of propagation along grain boundaries parallel to the applied stress, and the fact that the intergranular crack must propagate primarily in this direction accounts for the low susceptibility of longitudinally stressed specimens. The results suggest that the threshold stress for short transverse specimens approximates the low stress necessary to crack grain boundaries normal to the applied stress, and the threshold stress for longitudinal specimens approximates the high stress needed to propagate cracks along boundaries parallel to the applied stress. Preferred orientation was found to be of secondary importance when compared to the effect of grain morphology. A high degree of preferred orientation, rather than any specific slip plane orientation, was found to increase the susceptibility of specimens with the same grain morphology. Pitting corrosion was found to occur to a much greater extent on unstressed than on stressed (undergoing stress corrosion cracking) specimens. This phenomenon is explained by what is termed an "internal cathodic protection mechanism."

Wall, L. A., Flynn, J. H., Straus, S., **Rates of molecular vaporization of linear alkanes,** *J. Phys. Chem.* **74,** *17, 3237–3242 (1970).*

Key words: Alkanes; heats; *n*-hexatricontane; *n*-pristane; *n*-tetracosane; *n*-tetranonacontane, vaporization.

The rates of molecular vaporization of four linear alkanes, *n*-pristane (C_{19}), *n*-tetracosane (C_{24}), *n*-hexatricontane (C_{36}), and *n*-tetranonacontane (C_{94}) was measured. By both isothermal and nonisothermal methods, the kinetics of the vaporization process showed essentially zero order behavior as a vaporization process proportional to the surface area should. The Arrhenius slope plus $3\,RT/2$ was compared to heats of vaporization of other *n*-alkanes in the literature. The old and new data show that the heat of vaporization is proportional to the two-thirds power of the number, n, of carbon atoms in the species and not to the first power. The majority of the known heats of vaporization were well fitted by the equation,

$$\Delta H_v = 13.43\ n^{2/3} - 0.08075\ T + 12.22,\ \text{KJ/mol}$$

The tetranonacontane vaporized without detection of hydrocarbon decomposition products by mass spectral monitoring. The results suggests a much higher limit to the size of species capable of molecular vaporization without decomposition, than previously assumed.

West, E. D., Churney, K. L., **Theory of isoperibol calorimetry for laser power and energy measurements,** *J. Appl. Phys.* **41,** *No. 6, 2705–2712 (May 1970).*

Key words: Calorimetry; laser calorimetry; lasers; thermadynamics.

Laser power and energy measurements are commonly made in calorimeters operating in a constant-temperature environment. These calorimeters are analyzed in terms of the first law of thermodynamics and the boundary value problem describing heat flow in the calorimeter. This theory of the measurement suggest design features of the calorimeter, sources of error to be avoided in design and operation, and tests to demonstrate experimentally the adequacy of the design. The analysis shows how time-temperature data can be used to allow for the temperature gradient on the calorimeter and the heat exchange due to transients in the temperature.

Other NBS Publications

J. Res. Nat. Bur. Stand. (U.S.), 74C (Eng. and Instr.), Nos. 3&4 (July–Dec. 1970), SD Catalog No. C13.22/sec.C:74/3&4. $1.25.
Techniques for comparing four-terminal-pair admittance standards. R. D. Cutkosky.

Some applications for series impedance elements in radio frequency immittance measurements. L. E. Huntley.

A pulse heating method for the measurement of melting point of electrical conductors (thin wires) above 2000 K. A. Cezairliyan.

A time-shared computer system for diffractometer control. H. A. Alperin and E. Prince.

Tensile deformation of vapor-deposited copper reinforced with tungsten wires. W. D. Jenkins, W. A. Willard, and D. A. Harne.

"Connector-pair" techniques for the accurate measurement of two-terminal low-value capacitances. A. Millea.

The use of dew-point temperature in humidity calculations. A. Wood.

Bolovac application for HF and microwave power measurement and standardization. M. C. Selby.

Publications of the National Bureau of Standards.

Index to volume 74C, January–December 1970.

Borie, E., Radiative corrections to back scattering, Phys. Rev. C, **2,** No. 2, 770–771 (August 1970).

Candela, G. A., Spin relaxation process of chromium ion in potassium alum., J. Chem. Phys. **52,** No. 7, 3754–3757 (April 1, 1970).

Evans, W., Garvin, D., The evaluator versus the chemical literature, J. Chem. Doc. **10,** No. 3, 147–150 (1970).

Feldman, A., Brower, W. S., Jr., Horowitz, D., Optical activity and Faraday rotation in bismuth oxide compounds, Appl. Phys. Letters **16,** No. 5, 201–202 (March 1, 1970).

Feldman, A., Kahn, A. H., Landau diamagnetism from the coherent states of an electron in a uniform magnetic field, Phys. Rev. B, **1,** No. 12, 4584–4589 (June 15, 1970).

Frederikse, H. P. R., Comments on electronic transport in transition metal oxides, J. Res. Develop. **14,** No. 3, 295–300 (May 1970).

Hosler, W. R., Low resistance contacts on semiconducting oxides, Solid-State Electron. **13,** 517–519 (1970).

Howett, G. L., Achromatic-point prediction, J. Opt. Soc. Am. **60,** No. 7, 951–958 (July 1970).

Hubbell, J. H., X-ray absorption 75 years later, Phys. Bull. No. **21,** 353–357 (1970).

Hummer, D. G., Mihalas, D., Model atmospheres for the central stars of planetary nebulae, Monthly Notices Roy. Astron. Soc. **147,** No. 4, 339–354 (1970).

Hust, J. G., Thermal anchoring of wires in cryogenic apparatus, Rev. Sci. Instr. **41,** No. 5, 622–624 (May 1970).

Johnson, W. T. K., Chertok, B. T., Dick, C. E., Study of nuclear states of several odd-A nuclei $68 \leq Z \leq 79$ through electromagnetic excitation from 2.3 to 3.6 MeV, Phys. Rev. Letters **25,** No. 9, 599–602 (August 31, 1970).

Kasen, M. B., The effect of grain boundaries on the recovery of electrical properties during annealing, Scripta Met. **4,** 575–580 (1970).

Mann, D. B., Roder, H. M., Liquefied natural gas as a cryogenic fluid—instrumentation and properties (Proc. Transmission Conf. American Gas Association Operation Section, New Orleans, La., May 26–27, 1969), pp. T–98–T–106 (American Gas Association, Arlington, Va., 1970).

Meijer, P. H. E., O'Keeffe, D. J., Low-temperature behavior of a pure dipole-dipole system, Phys. Rev. B, **1,** No. 9, 3786–3800 (May 1, 1970).

Nimeroff, I., Deuteranopic convergence point, J. Opt. Soc. Am. **60,** No. 7, 966–969 (July 1970).

Phucas, C. B., Technical Standards Coordinator, Glass stopcocks with polytetrafluoroethylene (PTFE) plugs, Nat. Bur. Stand. (U.S.), Voluntary Prod. Stand. 28–70, 10 pages (Sept. 1970) 25 cents, SD Catalog No. C13.20/2:28–70.

Reed, R. P., Arp., V. D., Techniques for measuring stress, strain and resistivity at 4K for very soft materials. Cryogenics Letter to Editor, **9,** No. 5, 362–364 (October 1969).

Roder, H. M., Diller, D. E., Thermal conductivity of gaseous and liquid hydrogen, J. Chem. Phys. **52,** No. 11, 5928–5949 (June 1, 1970).

Searles, S. K., Sieck, L. W., Ausloos, P., Reactions of $C_2H_6^+$. Formation of the $(C_2H_6)_2^+$ ion, J. Chem. Phys. **53,** No. 2, 849–850 (July 15, 1970).

Searles, S. K., Sieck, L. W., High pressure photoionization mass spectrometry, III. Reactions of $NO^+(X'\Sigma^+)$ with C_3-C_7 hydrocarbons at thermal kinetic energies, J. Chem. Phys. **53,** No. 2, 794–797 (July 15, 1970).

Sharp, E. J., Weber, M. J., Cleek, G., Energy transfer and fluorescence quenching in Eu- and Nd-doped silicate glasses, J. Appl. Phys. **41,** No. 1, 364–369 (Jan. 1970).

Shinyayev, A. Ya., Butrymowicz, D. B., Interdiffusion in and the phase diagram for vanadium-rich alloys of the V-Al system at pressures 0 to 47 kbar, Met. Trans. **1,** No. 7, 1905–1907 (July 1970).

Stein, P. G., Lipkin, L. E., Shapiro, H. M., Spectre II: General-purpose microscope input for a computer, Science **166,** 328–333 (Oct. 17, 1969).

Straty, G. C., Prydz, R., The vapor pressure of liquid fluorine (Proc. 1969 Cryogenic Engineering Conf., June 16–18, 1969, Univ. of California, Los Angeles, Calif.), Chapter in Advances in Cryogenic Engineering **15,** Paper No. B–1, 36–41 (Plenum Press, Inc., New York, N.Y., 1970).

Sugar, J., Spectrum of doubly ionized thulium (Tm III), J. Opt. Soc. Am. **69,** No. 4, 454–466 (Apr. 1970).

Sugar, J., Configuration $4f^{13}5d$ of doubly ionized ytterbium, J. Opt. Soc. Am. **60,** No. 4, 571–572 (Apr. 1970).

Swartzendruber, L. J., Bennett, L. H., Clustering, cold work, and the Mössbauer effect doublet structure in Cu-Ni-Fe alloys, Physics Letters **31A,** No. 10, 581–582 (May 18, 1970).

Wilson, W. K., Fletcher, D. G., Paper research at the National Bureau of Standards, Indian Pulp Paper **24,** No. 7, 325–329 (Jan. 1970).

Wolcott, N. M., Falge, R. L., Jr., Cluster specific heat in $Cu_{0.6}Ni_{0.4}$ alloy, J. Low Temp. Phys. **2,** No. 314, 329–331 (1970).

Younglove, B. A., Measurements of the dielectric constant of saturated liquid oxygen (Proc. 1969 Cryogenic Engineering Conf., June 16–18, 1969, Univ. of California, Los Angeles, Calif.), Chapter in Advances in Cryogenic Engineering **15,** Paper No. C–3, 70–75 (Plenum Press, Inc., New York, N.Y., 1970).

**Publications with prices and SD Catalog numbers indicated may be purchased directly from the Superintendent of Documents, U.S. Government Printing Office, Washington, D.C. 20402 (foreign: one-fourth additional). NBS nonperiodical series are also available from the National Technical Information Service (NTIS) Springfield, Va. 22151 (formerly the Clearinghouse for Federal Scientific and Technical Information). Reprints from outside journals and the NBS Journal of Research may often be obtained directly from the authors.*

U.S. GOVERNMENT PRINTING OFFICE : OL 1971 — 413–992

OCT 40149
UNIVERSITY MICROFILMS INC
ATTN SERIALS SECTION
300 NORTH ZEEB RD
ANN ARBOR MICH 48106

UN
GOVERNME
PUBLIC DOCUMENTS DEPARTMENT
WASHINGTON, D.C. 20402

OFFICIAL BUSINESS

POSTAGE AND FEES PAID
U.S. GOVERNMENT PRINTING OFFICE

JOURNAL OF RESEARCH of the National Bureau of Standards
A. Physics and Chemistry

Vol. 75A, No. 2 March–April 1971

Contents

Page

Tentative set of key values for thermodynamics—Part I. Report of the ICSU–CODATA Task Group on Key Values for Thermodynamics, October, 1970. S. Sunner. 97

Expanded formulation of thermodynamic scaling in the critical region. Martin J. Cooper. 103

Table of spin-orbit energies for *p*-electrons in neutral atomic (core) *np* configurations. W. C. Martin 109

Heat capacities of *cis*-1,4-polyisoprene from 2 to 360 K. S. S. Chang and A. B. Bestul. 113

Combined low-pressure and high-pressure measurements of density and bulk modulus of aviation instrument oil and 2-methylbutane and their mixtures. James C. Houck and Peter L. M. Heydemann. 121

Crystal structure of $Ca_2Na_2(CO_3)_3$ (shortite). B. Dickens, A. Hyman, and W. E. Brown. 129

Publications of the National Bureau of Standards. 137

Library of Congress Catalog Card Number: 62-37059

For sale by the Superintendent of Documents, U.S. Government Printing Office, Washington, D.C. 20402. (Order by SD Catalog No. C 13.22/sec.A:75/2). Single copy price varies. This issue $1.25. Subscription price: $9.50 a year; $2.25 additional for foreign mailing.

UNITED STATES GOVERNMENT PRINTING OFFICE, WASHINGTON : 1971